J. Fluid Mech. (2005), *vol.* 535, *pp.* 65–100.
doi:10.1017/S0022112005004453 Printed in the United Kingdom

The generation of streaks and hairpin vortices from a localized vortex disturbance embedded in unbounded uniform shear flow

By VICTORIA SUPONITSKY[1]†, JACOB COHEN[1] AND PINHAS Z. BAR-YOSEPH[2]

[1]Faculty of Aerospace Engineering, Technion–IIT, Haifa, 32000, Israel

[2]Computational Mechanics Laboratory, Faculty of Mechanical Engineering, Technion–IIT, Haifa, 32000, Israel

(Received 18 February 2004 and in revised form 7 February 2005)

The similarity of the coherent structures (streaks and hairpin vortices) naturally occurring in different fully developed bounded turbulent shear flows as well as in transitional flows suggests the existence of a basic mechanism responsible for the formation of these structures, under various base flow conditions. The common elements for all such flows are the shear of the base flow and the presence of a localized vortical disturbance. The objective of the present numerical study is to examine the capability of a simple model of interaction, between a localized vortical disturbance and laminar uniform unbounded shear flow, to reproduce the generation mechanism and characteristics of the coherent structures that naturally occur in turbulent bounded shear flows. The effects of the disturbance 'localized character' in the streamwise and spanwise directions as well as its initial orientation relative to the base flow are investigated by using several geometries of the initial disturbance. The results demonstrate that a small-amplitude initial disturbance (linear case) eventually evolves into a streaky structure independent of its initial geometry and orientation, whereas, a large-amplitude disturbance (strongly nonlinear case) evolves into a hairpin vortex (or a packet of hairpin vortices) independent of its geometry over a wide range of the initial disturbance orientations. The main nonlinear effects are: (i) self-induced motion, which results in the movement of the vortical structure relative to the base flow and the destruction of its streamwise symmetry, and (ii) the alignment of the vortical structure with the vorticity lines. This is unlike the linear case, where there is a strong deviation of the vorticity vector from the direction of the vortical structure. Qualitatively, the disturbance evolution is sufficiently independent of its initial geometry, whereas the associated quantitative characteristics, i.e. inclination angle, centre and strength (which is governed by the transient growth mechanism), strongly depend on the disturbance geometry. The Reynolds number is found to have a negligible effect on the kinematics of the vortical structure, but does have a significant effect on its transient growth. Finally, the formation of the asymmetric hairpin vortex, due to minor spanwise asymmetries of the initial disturbance, is demonstrated.

† Present address: Department of Engineering, Queen Mary and Westfield College, University of London, Mile End Road, London. v.suponitsky@qmul.ac.uk

1. Introduction

1.1. *Coherent structures*

Wall-bounded turbulent shear flows are characterized by unsteady, seemingly chaotic motion. In fact, however, the motion is not random and it has been observed to be governed by well-organized vortical structures. These turbulent shear flows are known to consist mainly of two different kinds of coherent vortical structure: (i) counter-rotating streamwise vortices, which lead to the formation of low- and high-speed velocity regions (streaks), observed in the near wall region, and (ii) hairpin-shaped vortices extended across the boundary layer. The two kinds of coherent structure were first identified experimentally by Kline *et al.* (1967). Following their pioneering work, these vortical structures were reported by a growing list of workers who suggested them as basic flow elements of wall-bounded turbulent shear flows. The main experimental and numerical findings regarding the coherent structures are discussed and summarized in Robinson (1991) and Smith & Walker (1995) and also in §1 of Schoppa & Hussain (2002).

One of the remarkable features of these coherent structures, is that their characteristic length scales (expressed in wall units: $y^+ = yu^*/\nu$, $u^* = \sqrt{\tau_w/\rho}$) remain almost unchangeable for various kinds of shear flow and over a significant range of Reynolds numbers. In the above expressions, y is a dimensional length, ν is the kinematic viscosity, ρ is the fluid density and τ_w is the wall shear stress. The characteristic length of the streamwise vortices and the associated low-speed regions (streaks), has been found to be of the order of 600 to 1000 wall units, the diameter of the streamwise vortices is typically between 10 and 40 wall units and the mean spanwise streak spacing is about 100 wall units. (Kline *et al.* 1967; Kim, Kline & Reynolds 1971; Smith & Metzler 1983; Robinson 1991).

The hairpin-type vortical structures consist of a pair of counter-rotating legs joined by a relatively short 'head' segment. These vortices were found to be inclined at about 45° to the base flow direction, and remain identifiable even at high Reynolds numbers of the order of $Re_\theta \cong 10^4$, where θ is the momentum thickness (Head & Bandyopadhyay 1981). The spanwise separation of the two counter-rotating legs is about 50–60 wall units according to Wallace (1985), and does not exceed 100 according to other investigators (a complete table of the reported coherent structures characteristics can be found in Panton 1997). The convective velocity of the hairpin's head was measured by several investigators and appeared to be lower than the free-stream velocity even when the head was outside the boundary layer. The reported velocities are within the range of $0.4U_\infty - 0.8U_\infty$ (Panton 1997). Adrian, Meinhart & Tomkins (2000) using the particle image velocimetry (PIV) technique, indicated the existence of packets of hairpin vortices in turbulent boundary layer.

The evolutionary dynamics as well as the characteristic length scales have been found to be similar in both fully turbulent and transitional shear flows. Therefore, in order to understand the underlying physics of coherent vortical structures in wall-bounded turbulent shear flows, several authors have studied the evolution of similar structures artificially generated in sub-critical wall-bounded laminar shear flows. The advantage of this approach is that the flow is 'quiet' and therefore the vortical structure can be easily identified and followed. However, in this approach the influence of the turbulent Reynolds stress, associated with other vortical structures, is ignored.

Blackwelder (1983) compared the constituent elements of counter-rotating streamwise vortices for both transitional and turbulent boundary layers and suggested that

the dynamics of the vortices are similar, and their dimensions are comparable when scaled with viscous parameters, ν and u^*. In a subsequent work, Swearingen & Blackwelder (1987) experimentally studied the evolution of these vortices, generated via a Görtler instability mechanism along a concave wall. The authors reported that the spanwise wavelength and streamwise extent of the vortices compare favourably with those observed in transitional and turbulent flat-plate boundary layers when expressed in wall units.

Hairpin vortices (or horseshoe vortices) were also artificially generated in a laminar boundary layer. Comparison of the artificially generated hairpin vortices with the vortical structures observed in turbulent boundary layers showed striking similarities with regard to the details of the vortical shapes and their inclination angles to the main flow direction. Using a suction technique, hairpin vortices were generated in a laminar boundary layer by Acarlar & Smith (1987*b*) and in a rotating axisymmetric Couette flow by Levinski & Cohen (1995) and by Malkiel, Levinski & Cohen (1999). Haidari & Smith (1994) used a pulsed injection from a streamwise slot to generate hairpin vortices in a sub-critical laminar boundary layer, while Svizher & Cohen (2002) used a continuous injection to generate hairpin vortices in a sub-critical plane Poiseuille flow. Hairpin vortices were also generated behind a hemispherical bump by Acarlar & Smith (1987*a*). Some of the experimental results were confirmed and extended by numerical simulations. Numerical studies have been performed by Singer & Joslin (1994) for the experiments of Haidari & Smith (1994), by Rosenfeld, Cohen & Levinski (1999) for the experiments of Malkiel *et al.* (1999) and more recently, by Skote, Haritonidis & Henningson (2002) for the experiments of Acarlar & Smith (1987*b*).

1.2. *Regeneration mechanisms of turbulent structures*

One of the main objectives in the studies of coherent structures in fully developed turbulent flows, is to understand their self-generation ability. A variety of mechanisms describing the regeneration cycle has been proposed, and most of them can be roughly divided into two main categories (see Schoppa & Hussain 2002): parent–offspring mechanisms (i.e. the structure produces self-similar structures), or instability-based mechanisms (i.e. the structure produces a new class of structures).

Zhou, Adrian & Balachandar (1996) and Zhou *et al.* (1999) proposed an offspring regeneration mechanism in which the key element is a single strong hairpin vortex. In these works the evolution of a hairpin-like vortex structure (extracted from the low-Reynolds-number turbulent channel flow database (Kim, Moin & Moser 1987)) imposed on a mean turbulent channel flow was investigated using direct numerical simulation of the Navier–Stokes equations. They demonstrated that initial vortices, having vorticity that is weak relative to the mean vorticity, evolve gradually into Ω-shaped vortices which persist for long times and decay slowly. When the amplitude of the initial vortex exceeds a certain threshold relative to the mean flow, new hairpin vortices are generated upstream and downstream of the primary vortex, forming a coherent packet of hairpins. In this mechanism, the velocity field, induced by the parent vortex, generates intense local shear layers, mainly composed of spanwise vorticity. These shear layers roll-up into spanwise vortices which connect with the existing quasi-streamwise legs, and are stretched by the mean shear into offspring hairpin vortices, detached from the primary hairpin vortex.

Another offspring mechanism (implying that there is no coupling between the inner and outer layer dynamics) was suggested by Brooke & Hanratty (1993), who studied the spatio-temporal velocity field from DNS data. In this mechanism, an

opposite-signed offspring vortex forms underneath a parent vortex, whose downstream end has lifted from the wall. Similar findings were obtained by Bernard, Thomas & Handler (1993), who further noted that new vortices mainly formed from strong vertical vorticity component.

A detailed review of the instability-based mechanisms can be found in § 1 of Schoppa & Hussain (2002). Here the discussion is restricted to the 'streak-instability' based mechanisms. Robinson (1991) studied the evolution of instantaneous structures identified from DNS data and proposed, that low-speed streaks, generated by the streamwise vortices, contain a locally unstable $U(y)$ shear, which results in the generation of new spanwise vortices. One side of this spanwise vortex is stretched into a new quasi-streamwise vortex, which again generates a new streak closing the cycle. This $U(y)$ instability mechanism conceptually corresponds to varicose modes, which exhibit a hairpin-type perturbation symmetry.

Hamilton, Kim & Waleffe (1995) applied the 'minimal flow unit' concept of Jimenez & Moin (1991) to plane Couette flow to study the streak instability concept. Accordingly, the spanwise width of the computational domain corresponded closely to the typical observed spanwise spacing of near-wall streaks, and its further decreasing resulted in laminarization of the flow. They observed a well-organized process of near-wall structure regeneration, composed of three steps: formation of streaks by streamwise vortices; breakdown of streaks; and formation of new streamwise vortices. The regeneration cycle in turbulent channels flows at moderate Reynolds numbers was studied by Jimenez & Pinelli (1999) using direct numerical simulations. It was found that there is no coupling between the inner and outer regions, and a regeneration cycle in the near-wall region is similar to that of Hamilton *et al.* (1995). Based on the fact that the regeneration cycle resided above the viscous sub-layer, they suggested that a similar mechanism, may be active in other shear flows, particularly in the logarithmic layer. They also reported that the effect of the secondary vorticity generated at the wall, on the regeneration cycle is minor. Consequently, they suggested that the role of the wall is mainly to maintain the base shear.

Schoppa & Hussain (2002) proposed that the generation of streamwise vortices is governed by streak transient growth mechanism rather then by normal-mode instability. Their analysis of streaks extracted from fully developed near-wall turbulence showed that only about 20 % of the streaks exceed the strength threshold for developing linearly unstable sinuous modes. Therefore, they proposed that streamwise vortices are generated from more numerous streaks which are stable to normal modes.

1.3. *Transitional flows*

The similarity between vortical structures existing in fully developed turbulent shear flow and transitional flow suggests the similarity of the mechanisms responsible for their formation and subsequent dynamics. Therefore, certain aspects of laminar–turbulent transition are closely connected to the study of the dynamics of fully developed turbulent shear flows.

Inviscid theory (mainly due to Rayleigh 1880) predicts that velocity profiles with an inflection point may have exponentially growing eigenmodes. When the Reynolds number is finite, an additional class of eigenmodes (commonly referred to as Tollmien–Schlichting waves) may grow exponentially owing to viscous effects. If exponentially growing solutions do not exist, the flow is considered to be stable according to the linear stability theory (e.g. plane Couette flow, pipe Poiseuille flow). However, experiments have shown that transition may occur for Reynolds numbers as low as 280 for plane Couette flow (see e.g. Leutheusser & Chu 1971; Tillmark & Alfredsson

1992; Dauchot & Daviaud 1995) and 1760 for pipe Poiseuille flow (see e.g. Reynolds 1883; Leite 1959; Wygnanski & Champagne 1973; Darbyshire & Mullin 1995).

A possible non-modal growth mechanism was first proposed by Ellingsen & Palm (1975). They introduced an infinitesimal streamwise independent disturbance having a spanwise structure in a shear layer. They showed that for the inviscid flow, the disturbance streamwise velocity component can increase linearly with time, generating low- and high-speed streaks. As was shown by Landahl (1980), this growth is associated with the lift-up of fluid particles which retain their horizontal momentum as they move in the direction of the shear, causing perturbation in the streamwise velocity component. This inviscid growth together with viscous damping constitutes what is called a *transient growth* mechanism. Much work has been done on the lift-up and transient growth mechanisms (Hultgren & Gustavsson 1981; Boberg & Brosa 1988; Gustavsson 1991; Butler & Farrell 1992; Henningson, Lundbladh & Johansson 1993; Reddy & Henningson 1993; Ben-Dov, Levinski & Cohen 2003), demonstrating a considerable linear amplification of a three-dimensional disturbance before it decays owing to viscous effects. Streamwise vortices were found to lead to maximum spatial transient growth in a non-parallel flat-plate boundary-layer flow (Andersson, Berggren & Henningson 1999; Luchini 2000). If the amplitude of the streaks (associated with these vortices) reaches a sufficiently large value, secondary instabilities may occur which lead to early breakdown and transition (e.g. Elofsson & Alfredsson 1998, Andersson *et al.* 2001; Asai, Minagawa & Nishioka 2002).

The transient growth mechanism is also relevant for disturbances which are localized in the streamwise and spanwise directions, although the associated growth rate is slower than that of the streamwise independent disturbances (for comparison see the introduction of Bech, Henningson & Henkes 1998). The evolution of such disturbances in a laminar boundary layer over a flat plate was studied numerically and experimentally by Breuer & Haritonidis (1990) and Breuer & Landahl (1990) for small- and moderate-amplitude disturbances, respectively. Henningson *et al.* (1993) and Bech *et al.* (1998) used direct numerical simulations to study the evolution of localized disturbances in plane Poiseuille flow and in adverse and zero-pressure-gradient boundary layers, respectively. According to these studies, the disturbance may be viewed as consisting of two parts: a dispersive part (represented by the solutions to the Rayleigh equation) and a transient part travelling at the local mean velocity. The balance between these two parts is governed by the instability characteristics of the mean velocity profile. Furthermore, small-amplitude disturbances evolved into low- and high-speed streaks similar to those observed in turbulent flows, whereas moderate-amplitude disturbances developed into vortical structures resembling the three-dimensional lambda vortices which were observed in previous studies.

In all of the above studies, the Reynolds number was based on the parameters of the base flow, whereas the parameters of the initial disturbance were not taken into account. Furthermore, the characteristic length scales of the initial disturbances were at least comparable with that of the base flow (e.g. the boundary-layer thickness). The disturbance initial amplitude was defined as the ratio between the initial normal velocity component and the characteristic velocity of the base flow.

Levinski & Cohen (1995) proposed a general model characterizing the evolution of a localized (in all three dimensions) disturbance, the dimensions of which are much smaller than the characteristic length scale of the external shear flow. According to their model, a simple feedback mechanism takes place: the lift-up of the disturbance in the vertical direction stretches the external spanwise vorticity field and generates a disturbed vorticity component in the vertical direction. The direct effect of the external

shear flow is to rotate the disturbed vortex back towards the wall and thereby to amplify the streamwise vorticity component. The new streamwise vorticity component induces an additional vertical velocity which further enhances the lift-up effect and closes the feedback loop.

Finally, Shukhman & Levinski (2003) obtained an analytic solution of the linearized vorticity equation for the evolution of such a localized small-amplitude 'Gaussian vortex' (spherical vortex ring with Gaussian vorticity distribution) in an unbounded uniform shear flow.

1.4. *Present research*

The similarity of the coherent structures (streaks and hairpin vortices) naturally occurring in different fully developed bounded turbulent shear flows as well as in transitional flows suggests the existence of a basic mechanism responsible for the formation of these structures, under various base flow conditions. The common elements for all such flows are the shear of the base flow and the presence of a localized vortical disturbance. The objective of the present numerical study is to examine the capability of a simple model of interaction, between a localized vortical disturbance and laminar uniform unbounded shear flow, to reproduce the generation mechanism and characteristics of the coherent structures that naturally occur in turbulent bounded shear flows.

The term 'localized disturbance' referred to disturbances, the dimensions of which are much smaller than a typical scale representing the velocity gradient of the external flow. The role of the wall in this model is only to maintain the shear of the base flow, and to generate the initial disturbance, whereas its effect on the disturbance evolution is required to be negligible (Levinski & Cohen 1995). Obviously, the main advantages of this model are its relative simplicity and generality. As such, it is relevant to various fields: structure of turbulent boundary layers, by-pass transition to turbulence, and vortex dynamics.

The rest of the paper is organized as follows. The problem statement, including the definition of the initial disturbance, description of the governing parameters, definition of the vortical structure characteristics and the computational procedure, is given in § 2. The results are presented in § 3, which is subdivided into §§ 3.1–3.3, each describing the disturbance evolution having a different initial geometry. Section 3.1, is further subdivided into §§ 3.1.1–3.1.3 in which various effects of the governing parameters are addressed. The main results and related issues are discussed in § 4 and the main conclusions are given in § 5.

2. Problem statement

2.1. *The initial disturbance*

In general, any localized vortex (in all three dimensions) with a divergent free vorticity field can be used as an initial disturbance. In this study, three different geometrical shapes of the initial disturbance (all of them having a Gaussian vorticity magnitude distribution) are considered. The first one is a 'spherical' vortex ring with a Gaussian vorticity distribution, referred to as a 'Gaussian vortex', that is defined by the following equation:

$$\boldsymbol{\omega} = -\boldsymbol{p} \times \nabla F, \quad F = \left(\pi^{1/2}\delta\right)^{-3} \exp\left(-r_s^2/\delta^2\right), \tag{2.1}$$

where $\boldsymbol{\omega}$ is the vorticity vector, $\boldsymbol{p}$ is a vector defining its space orientation, r_s is a spherical radial coordinate, and δ is a representative length scale of the disturbance

(the disturbance maximum vorticity magnitude is obtained at $r_s = \delta/\sqrt{2}$). The function F in (2.1) is normalized such that its volume integral is equal to 1, ($\int_V F\,\mathrm{d}V = 1$). In this case the vector $\boldsymbol{p}$ is the fluid impulse of the initial vortical disturbance, defined as (e.g. Batchelor 1967):

$$\boldsymbol{p} = \tfrac{1}{2}\int_V \boldsymbol{r} \times \boldsymbol{\omega}\,\mathrm{d}V, \tag{2.2}$$

where $\boldsymbol{r}$ is the position vector. This disturbance, having a single length scale, serves as an example of a localized region of concentrated vorticity, with vorticity lines forming circles in a plane perpendicular to the direction of the fluid impulse vector $\boldsymbol{p}$.

The second shape of the initial disturbance is that of a horizontal streamwise elongated Gaussian vortex. It is defined by two characteristic length scales, allowing us to examine the effect of the disturbance streamwise elongation. Its vorticity field is also defined by (2.1), except for the spherical radial coordinate r_s which is replaced by r_e, the expression for which is given by:

$$r_e = \sqrt{\bar{x}^2 + y^2 + z^2}, \quad \bar{x} = \begin{cases} x - L; & |x| > L, \quad x > 0, \\ x + L; & |x| > L, \quad x < 0, \\ 0; & |x| < L, \end{cases} \tag{2.3}$$

where x, y and z are the streamwise, normal and spanwise directions, respectively, and L is a second characteristic length scale associated with the streamwise elongation of the disturbance. The disturbance initial elongation is determined by the length scales ratio L/δ. When this ratio is equal to zero, the initial disturbance reduces to that of the Gaussian vortex (equation (2.1)), whereas for a sufficiently large ratio, it can be approximately considered as a 'streamwise independent' disturbance.

The third shape of the initial disturbance is a toroidal vortex, also having two characteristic length scales. For a horizontal (x, z-plane) torus the vorticity field is given by:

$$\boldsymbol{\omega} = \begin{Bmatrix} z \\ 0 \\ -x \end{Bmatrix} A\,\exp(-y^2/\delta^2)\exp(-(r - r_o)^2/\delta^2), \tag{2.4}$$

where A is a positive constant defining the strength of the disturbance, $r = \sqrt{x^2 + z^2}$ is a radial cylindrical coordinate and r_o and δ are two characteristic length scales associated with the radius and the thickness of the torus, respectively. This initial disturbance has a vorticity distribution similar to that of the Gaussian vortex (for the horizontal torus, the vorticity lines form circles in the x, z-plane), however, the existence of two characteristic length scales allows us to vary the localized properties of the disturbance and seek the 'optimal' aspect ratio, for which the disturbance growth is maximal. From (2.1), it can be seen that the vorticity magnitude for the Gaussian vortex is proportional to:

$$||\boldsymbol{\omega}|| \sim r_s \exp\left(-r_s^2/\delta^2\right), \tag{2.5}$$

whereas for the toroidal disturbance, it is given by:

$$||\boldsymbol{\omega}|| \sim r\exp(-y^2/\delta^2)\exp(-(r - r_o)^2/\delta^2). \tag{2.6}$$

For $r_o = 0$, the distribution of the vorticity magnitude given by (2.6) is reduced to that of the Gaussian vortex (equation (2.5)), except that r_s and r in both expressions refer to the spherical and radial coordinates, respectively. Thus, the Gaussian disturbance can be considered as an approximate limit of the toroidal disturbance.

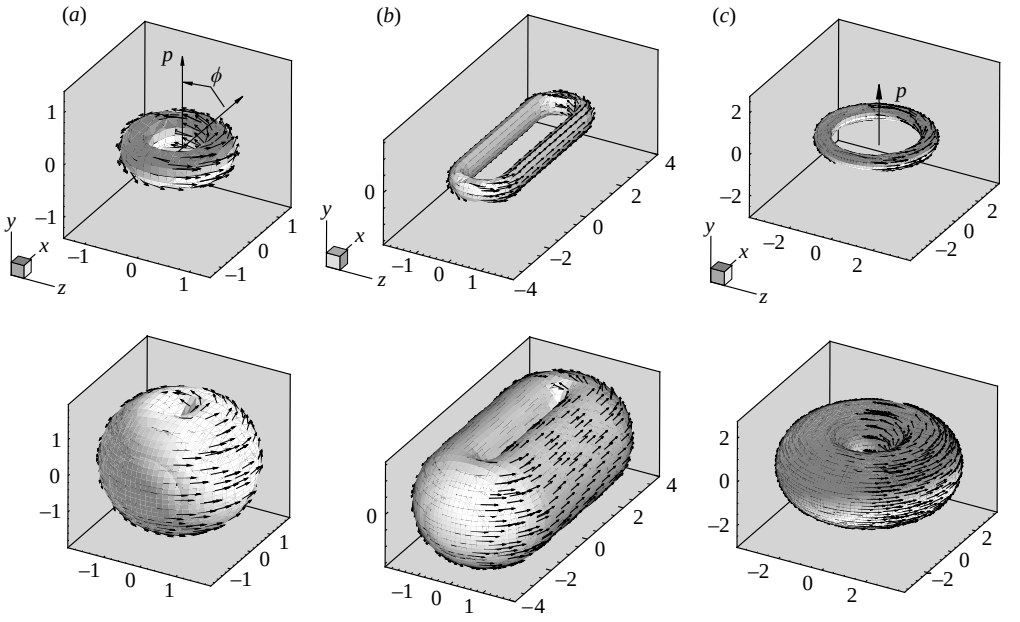

FIGURE 1. Iso-surfaces of the vorticity magnitude and the associated vorticity vectors of horizontal initial disturbances; (*a*) Gaussian vortex; (*b*) streamwise elongated disturbance with $L/\delta = 2$; (*c*) toroidal disturbance with $r_o/\delta = 2$. First row: $||\boldsymbol{\omega}||/\omega_{max} = 0.9$; Second row: $||\boldsymbol{\omega}||/\omega_{max} = 0.1$.

Examples of an initially horizontal Gaussian vortex (figure 1*a*), a streamwise elongated disturbance having a length scales ratio of $L/\delta = 2$ (figure 1*b*) and a toroidal disturbance having a length scales ratio of $r_o/\delta = 2$ (figure 1*c*) are presented by iso-surfaces of the normalized (with respect to its maximum ω_{max}) vorticity magnitude for two (high and low) threshold levels. To further clarify the structure of the vorticity field, the associated vorticity vectors are also shown by the black arrows. For the Gaussian and the streamwise elongated Gaussian disturbances, a detailed investigation of the disturbance evolution is presented. For the sake of completeness, only main results associated with the toroidal disturbance are given (more details concerning this case can be found in Suponitsky, Cohen & Bar-Yoseph 2004).

2.2. *Governing parameters*

Once the shape of the initial vortical disturbance is chosen, there are three parameters that govern the flow. The first one is the strength of the initial disturbance (ε) which is defined by the amplitude ratio between the maximum vorticity of the disturbance and the shear of the base flow (Ω), i.e.

$$\varepsilon = \omega_{max}/\Omega. \tag{2.7}$$

As in the present problem statement, a characteristic velocity of the base flow does not exist, the proper definition of the disturbance amplitude is given in terms of the vorticity ratio. When the amplitude of the disturbance is small ($\varepsilon \ll 1$) the problem is considered to be a 'linear' one.

The second governing parameter is the orientation of the initial disturbance relative to the direction of the base flow. This is given in terms of the angle ϕ, between the

direction of the fluid impulse vector $\boldsymbol{p}$ and the positive direction of the x-axis (figure 1a). For the initially horizontal disturbance, the fluid impulse vector is $\boldsymbol{p}=(0,\, p_y,\, 0)$ and the corresponding angle is $\phi=90^\circ$.

The third governing parameter is the Reynolds number, which for the case of a Gaussian vortex disturbance is defined as:

$$Re = \Omega\delta^2/\nu. \tag{2.8}$$

This definition represents the ratio between the time scale associated with the shear of the base flow ($1/\Omega$) and the viscous time scale (δ^2/ν). For the elongated and toroidal disturbances, the characteristic length scale δ (associated with the thickness of the vortical region) is also used for the Reynolds number definition, and the disturbance geometry is defined by the length scales ratios L/δ and r_o/δ, respectively.

All variables are made dimensionless using δ and $1/\Omega$ reference length and time scales, respectively. Accordingly, $X=x/\delta,\ Y=y/\delta,\ Z=z/\delta$ and $T=t\Omega$.

2.3. *Vortex identification and characteristics*

2.3.1. *Vortex identification*

One of the most natural ways to identify a vortical structure is to use various threshold levels of the vorticity magnitude iso-surfaces. However, the use of this method is somewhat subjective as the shape of the vortical structure strongly depends on the chosen threshold level (e.g. figure 1). Several definitions for vortex identification, based on the properties of the velocity gradient tensor ∇u, have recently been proposed. Hunt, Wray & Moin (1988) defined an 'eddy' as the region with positive second invariant, Q, of the velocity gradient tensor, with the additional condition that the pressure be lower than the ambient value. Chong, Perry & Cantwell (1990) proposed that a vortex core is a region with complex eigenvalues of ∇u; complex eigenvalues imply that the local streamline pattern is closed or spiral in a reference frame moving with the point. Complex eigenvalues will occur when the discriminant ($\triangle$) is positive. Jeong & Hussain (1995) defined a vortex core as a connected region with $\lambda_2<0$, where $\lambda_1\geqslant\lambda_2\geqslant\lambda_3$ are the eigenvalues of the tensor $S^2+\hat{\Omega}^2$ (S and $\hat{\Omega}$ are the symmetric and antisymmetric components of the velocity gradient tensor, respectively).

In the present study, all of the methods mentioned above were applied to educe the vortical structure (for details see Suponitsky, Cohen & Bar-Yoseph 2003a). The results showed that the educed structure (according to the definitions based on the velocity gradient tensor) were not too sensitive to the chosen threshold levels and to the particular definition used. In the following, we use the vorticity magnitude iso-surfaces together with the Q definition for the identification of the vortical structure.

The purpose of the definitions based on the velocity gradient tensor is to extract regions of swirling motion. As such, the use of these definitions does not provide any information regarding the existence of vorticity sheets. These may be of relevance for understanding better the underlying physics associated with the coherent structures (see § 3). Finally, it is worth mentioning that regions confined by vorticity magnitude iso-surfaces as well as regions confined by surfaces based on the velocity gradient tensor, represent regions of concentrated vorticity and swirling motion, respectively. The swirl direction within the confined regions is, however, not known. For this, the corresponding distributions of the vorticity components must be provided as well.

2.3.2. *Vortex strength*

The strength of the vortical disturbance (W) is measured by integrating the enstrophy over the entire volume, i.e.

$$W(t) = \int_V ||\boldsymbol{\omega}(t)||^2 \, \mathrm{d}V. \tag{2.9}$$

The advantages of using the enstrophy integral (W) are due to its rapid convergence and its integral character, combining the strength of the vorticity field together with the disturbance geometrical size.

2.3.3. *Vortex centre, velocity and inclination angle*

Once the vortical structure is identified, its geometrical characteristics have to be defined. The first one is the centre of the vortical structure (CVS) which is defined as the first moment of enstrophy divided by the total enstrophy (analogous to the definition of 'centre of gravity'):

$$X_i(t) = \left[\int_V ||\boldsymbol{\omega}(t)||^2 x_i \, \mathrm{d}V \right] / W(t). \tag{2.10}$$

Subsequently, the velocity of the vortical structure can be defined as the velocity of its centre: $u_i(t) = \mathrm{d}X_i/\mathrm{d}t$.

Another geometrical parameter which is important for the description of the vortex evolution is the instantaneous inclination angle of the vortical structure relative to the base flow. Here this angle is defined with the aid of the tensor of enstrophy distribution (TED), which has been introduced by Shukhman & Levinski (2003). The TED is defined as follows:

$$T_{ij}(t) = \int_V ||\boldsymbol{\omega}(t)||^2 (x_i - X_i(t))(x_j - X_j(t)) \, \mathrm{d}V, \tag{2.11}$$

where $X_i(t)$, $i = 1, 2, 3$ are the coordinates of the CVS defined by (2.10). Since the TED is a symmetric tensor, its principal axes can be calculated. The largest eigenvalue corresponds to the principal axis in the vortex plane, along which the vortex is extended the most. The tensor's smallest eigenvalue corresponds to the shortest principal axis. The direction of this axis is perpendicular to the vortex plane. A schematic drawing of the principal axes, calculated from the TED and the definition of the inclination angle α is shown in figure 2. For a disturbance, which is symmetric with respect to the plane $Z = 0$ (which is the main focus of the present work), the expression for α is given by (Shukhman & Levinski 2003):

$$\alpha = \tfrac{1}{2} \arctan\left(\frac{2T_{12}}{T_{11} - T_{22}} \right) + \tfrac{1}{4}\pi(1 + s) - \tfrac{1}{2}\pi, \quad s = \mathrm{sign}(T_{11} - T_{22}). \tag{2.12}$$

The angle α is used as a measure of the vortical structure inclination angle, whenever it correlates well with the visual inclination angle.

2.4. *Numerical procedure*

The commercial CFD code 'FLUENT' based on the finite-volume method is used for the solution of the full Navier–Stokes equations for the primitive variables. The schematic of the computational domain (for the 'Gaussian vortex' disturbance) and the coordinate system definition is shown in figure 3. Along the streamwise direction (x) the periodic boundary conditions are employed. The moving-walls boundary

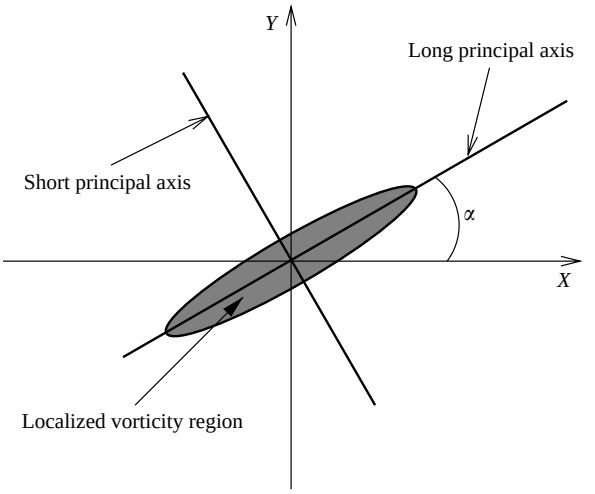

FIGURE 2. A schematic drawing of the principal axes calculated from the TED.

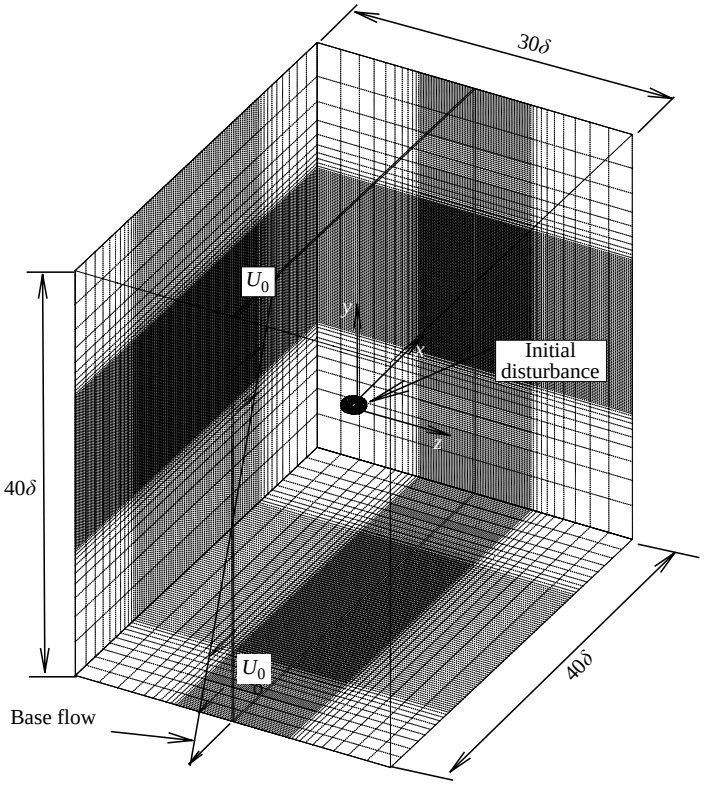

FIGURE 3. Schematic drawing of the computational domain (x-streamwise direction; y-transverse direction; z-spanwise direction).

conditions are imposed in the walls-normal direction (y). Accordingly, $u(y = 20\delta) = U_0$ and $u(y = -20\delta) = -U_0$. For the 'Gaussian vortex' disturbance, the size of the whole computational domain is $40\delta \times 40\delta \times 30\delta$ along the x, y and z directions, respectively. The size of the inner region surrounding the disturbance is $20\delta \times 14\delta \times 10\delta$. The whole

computational domain has about one million grid nodes. For the streamwise elongated disturbances, the size of the computational domain is extended to $80\delta \times 30\delta \times 50\delta$ and the whole computational domain has about 1.3 million grid nodes. For both computational grids, the resolution in the region surrounding the vortical structure is similar, and is equal to 5–6 volume elements per disturbance length scale δ in all directions. This size of the computational domain is sufficiently large (relative to the size of the initial disturbance), so that the effect of the finite computational domain on the disturbance development is negligible. For the spanwise symmetric initial disturbances ($p_z = 0$), the vortical structure remains symmetric around the $Z = 0$ plane during the entire evolution (see §§ 3.1.3 and 3.1.4). Thus, the computations are carried out on half of the computational domain with the symmetry boundary condition imposed on the $Z = 0$ plane.

The initial total velocity field, $\boldsymbol{U}_{total}$, is the sum of two contributions: the uniform base shear flow (figure 3), and the disturbed velocity field $\boldsymbol{u}$. The uniform shear base flow velocity profile ($\boldsymbol{U}_{base} = (\Omega y, 0, 0)$) is obtained numerically as a steady-state solution of the laminar two-dimensional Couette flow with zero pressure gradient. The initial vortical disturbance is placed at the centre of the computational domain. Because the initial disturbance is given in terms of its vorticity field, the corresponding velocity distribution must first be calculated in order to provide the initial velocity field required for the CFD code. For the particular case in which the disturbance is described by the function $F = F(r_s)$ (equation (2.1)), an analytic velocity distribution exists (Shukhman & Levinski 2003):

$$u_i = F(r_s)\left[p_i - \frac{x_i(\boldsymbol{p}\cdot\boldsymbol{r_s})}{r_s^2}\right] - \frac{H(r_s)}{r_s^3}\left[p_i - \frac{3x_i(\boldsymbol{p}\cdot\boldsymbol{r_s})}{r_s^2}\right], \tag{2.13}$$

where $H(r_s) = \int_0^{r_s} F(\xi)\xi^2\,\mathrm{d}\xi$ and $u_i(0) = 2p_i/3$.

For the toroidal disturbance (equation (2.4)), the corresponding velocity field is given by (Batchelor 1967):

$$\boldsymbol{u}(x, y, z) = -\frac{1}{4\pi}\int_V \frac{\boldsymbol{s}\times\boldsymbol{\omega}'}{s^3}\,\mathrm{d}V', \tag{2.14}$$

where $\boldsymbol{s} = (x - x', y - y', z - z')$ and $s = ||\boldsymbol{s}|| = \sqrt{(x-x')^2 + (y-y')^2 + (z-z')^2}$.

For most of the simulations, the size of the initial vortical disturbance and the shear of the base flow are $\delta = 1$ mm and $\Omega = 40\,\mathrm{s}^{-1}$, respectively. These parameters are chosen in accordance with the experiments of Malkiel *et al.* (1999) carried out in a (water) Taylor–Couette apparatus. For this set of parameters, the relevant Reynolds number is $Re = \Omega\delta^2/\nu = 40$.

The validation of the results was carried out by comparing our numerical results for the case of a small amplitude ($\varepsilon \ll 1$) Gaussian vortex disturbance with the analytic solution of the three-dimensional linearized vorticity equation which was recently obtained by Shukhman & Levinski (2003) (see Suponitsky *et al.* 2004). Tests for the time and grid resolutions were carried out as well (Suponitsky 2003).

3. Results

3.1. *Gaussian vortex disturbance*

3.1.1. *The effect of the initial disturbance amplitude*

In this section, the temporal evolution of a Gaussian vortex disturbance having a spanwise symmetry ($p_z = 0$ in (2.1)) and a characteristic Reynolds number of $Re = 40$

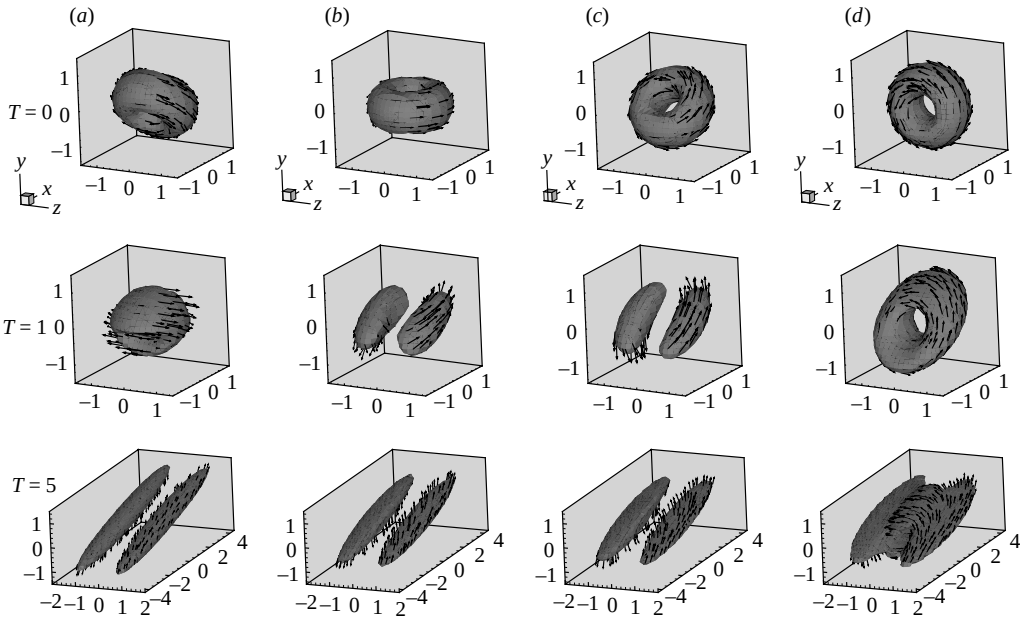

FIGURE 4. Evolution of a small-amplitude ($\varepsilon = 0.015$) disturbance; iso-surfaces of the vorticity magnitude for $||\boldsymbol{\omega}||/\omega_{max} = 0.7$ and associated vorticity vectors indicated by the black arrows. (*a*) $\phi = 45°$; (*b*) $\phi = 90°$; (*c*) $\phi = 135°$; (*d*) $\phi = 180°$.

(equation (2.8)) is studied. The base flow field is antisymmetric with respect to the $Y = 0$ plane. Therefore, to cover all possible initial orientations of the disturbance, it is sufficient to vary the angle ϕ (figure 1*a*) within the range of $0 < \phi \leqslant 180°$. The evolution of initial disturbances having four representative initial orientations is considered: (i) a horizontal vortex ($\phi = 90°$, $\boldsymbol{p} = (0, |p_y|, 0)$), (ii) a vertical vortex ($\phi = 180°$, $\boldsymbol{p} = (-|p_x|, 0, 0)$), (iii) a vortex inclined at 45° relative to the base flow ($\phi = 135°$, $\boldsymbol{p} = (-|p_x|, |p_y = p_x|, 0)$), and (iv) a vortex inclined at 135° relative to the base flow ($\phi = 45°$, $\boldsymbol{p} = (|p_x|, |p_y = p_x|, 0)$). The evolutions of linear ($\varepsilon = 0.015$) and strongly nonlinear ($\varepsilon = 7.5$) initial disturbances, corresponding to the above mentioned initial orientations, are presented in figures 4 and 5, respectively by the iso-surfaces of the vorticity magnitude. Also presented are the associated vorticity vectors, indicated by the black arrows.

We can see that at long times ($T = 5$) the shapes of structures evolving from the small-amplitude disturbances (figure 4) are almost independent of the disturbance initial orientation, and consist of a pair of counter-rotating quasi-streamwise vortices. For the vortical structure evolving from the vertical ($\phi = 180°$) initial disturbance, top and bottom vorticity sheets, bridging the pair of quasi-streamwise vortices, can be also seen. It should be noted that these vorticity sheets are part of the long time evolving structure. These could have been observed in all other orientations as well, if a lower threshold level had been used (for more details see Suponitsky *et al.* 2003*a*, *b*). The evolution of the disturbances having $\phi = 90°$ and $\phi = 135°$ initial orientations is quite similar, both of them quickly evolve (by $T = 1$) into a pair of counter-rotating vortices, which later on just stretch out (mainly) along the streamwise direction. For the initial vertical disturbance ($\phi = 180°$), it takes a longer time to reach the state of the resulting structure. During its evolution, it simultaneously undergoes rotation and

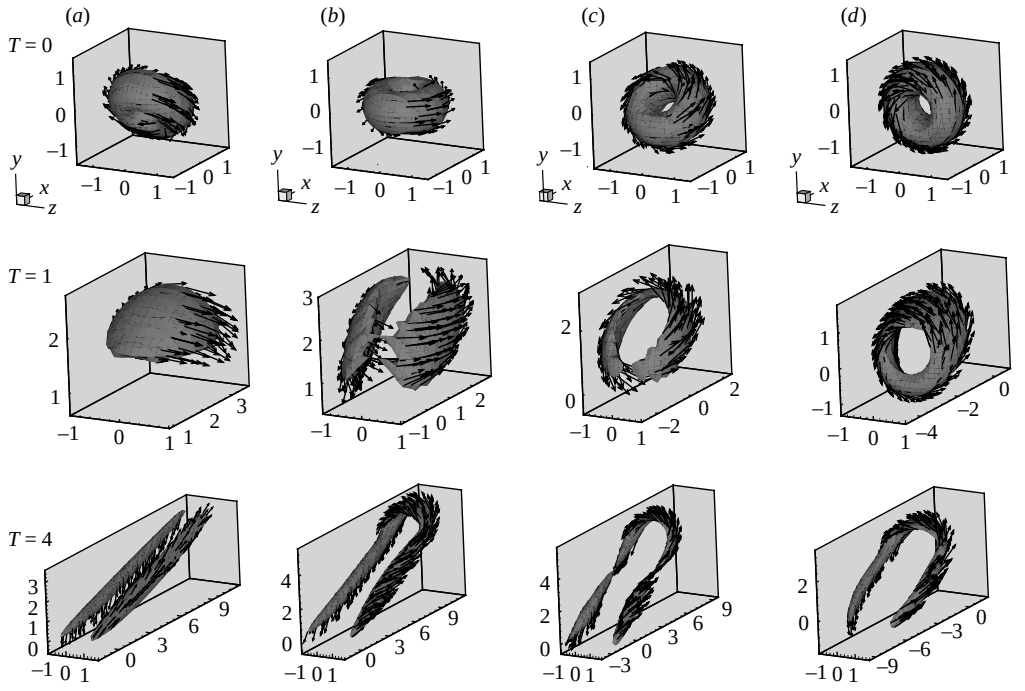

FIGURE 5. Evolution of a large-amplitude ($\varepsilon = 7.5$) disturbance; iso-surfaces of the vorticity magnitude for $||\boldsymbol{\omega}||/\omega_{max} = 0.7$ and associated vorticity vectors. (*a*) $\phi = 45°$; (*b*) $\phi = 90°$; (*c*) $\phi = 135°$; (*d*) $\phi = 180°$.

stretching. The evolution of a disturbance, which has an initial orientation of $\phi = 45°$, is governed mainly by stretching (i.e. the long principal axis does not rotate; instead the short one is stretched out and becomes the long principal axis).

In the nonlinear case (figure 5), the disturbances having initial orientations of $\phi = 90°, 135°$ and $180°$ evolve into hairpin shape vortices by $T = 4$. Although there are some differences in their geometrical shapes, the basic structure of the vortical structure is the same, consisting of two vortical legs joined together by a relatively short quasi-spanwise vortex head. The resulting vortical structure developed from a large-amplitude disturbance having an initial orientation of $\phi = 45°$, is similar to the structure evolved from a small-amplitude disturbance (figure 4*a* at $T = 5$).

To clarify the evolution process, the projections on the x, y-plane of the iso-surfaces presented in figures 4 and 5 are shown in figures 6 and 7 for the linear and strongly nonlinear disturbances, respectively. The long principal axis, calculated from the tensor of enstrophy distribution (TED), is shown by the black solid line together with the associated velocity vectors at the $Z = 0$ plane (the location of maximum velocity) which are indicated by the black arrows. The corresponding distributions of the streamwise and vertical velocity components along the long principal axis at the $Z = 0$ plane (plotted by solid and dotted lines, respectively), are added underneath the corresponding vorticity iso-surfaces. It can be seen that the direction of the long principal axis corresponds well to the visual inclination angle of the vortical structure for all orientations of the linear initial disturbance (figure 6) and for most orientations, and in particular the $\phi = 90°$ and $\phi = 135°$ cases, of the strongly nonlinear (figure 7) disturbances during the entire evolution.

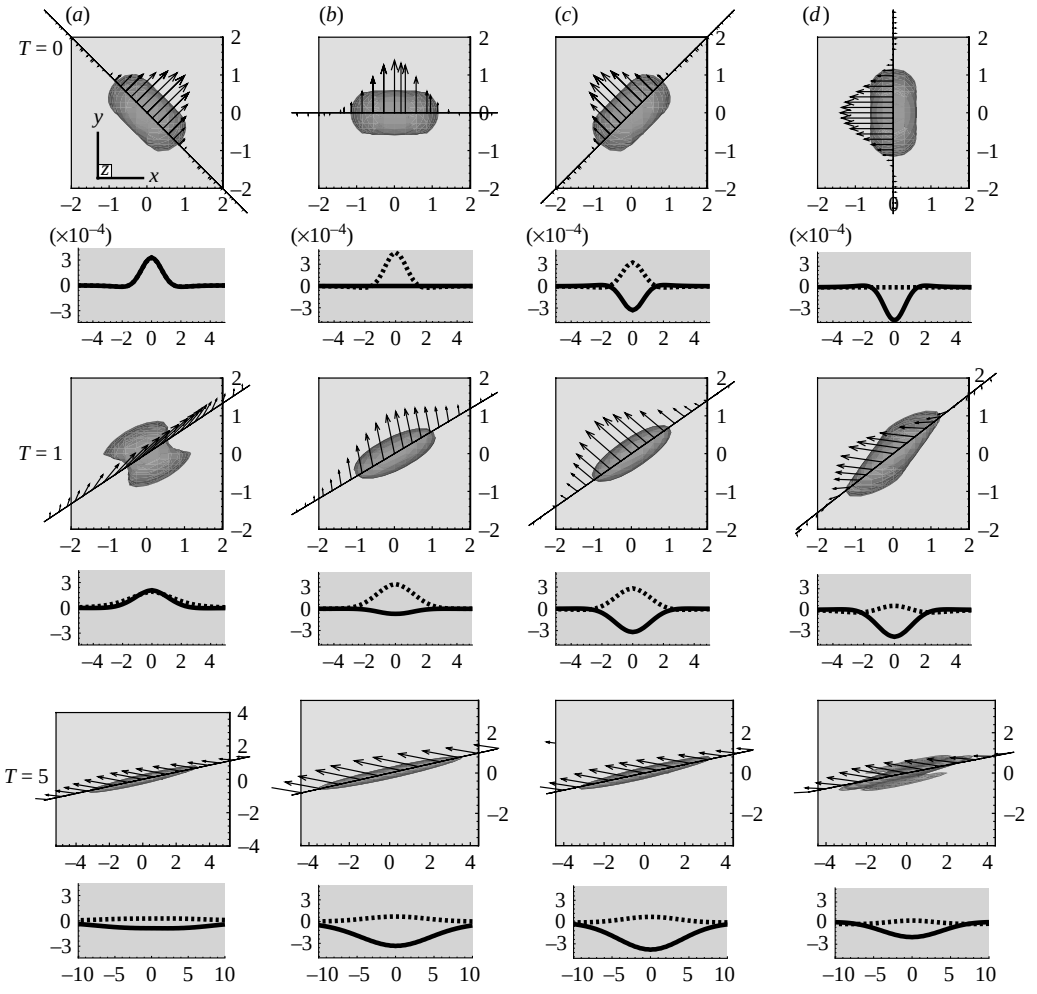

FIGURE 6. Evolution of a small-amplitude ($\varepsilon = 0.015$) disturbance. Odd rows: projection of the iso-surfaces of the vorticity magnitude for $||\boldsymbol{\omega}||/\omega_{max} = 0.7$ on the (x, y)-plane, long principal axis (black line), velocity vectors along the principal axis at the $Z = 0$ plane. Even rows: streamwise (solid) and vertical (dotted) velocity components ($\mathrm{m\,s^{-1}}$) distributions along the long principal axis at the $Z = 0$ plane. (The units along the abscissa correspond to $X/|\cos\alpha|$.) (*a*) $\phi = 45°$; (*b*) $\phi = 90°$; (*c*) $\phi = 135°$; (*d*) $\phi = 180°$.

Figure 6 shows that by $T = 1$, the extracted vortical structures developed from the disturbances having $\phi = 90°$ and $\phi = 135°$ initial orientations, are very similar. However, the corresponding directions of their associated induced velocity are different. At long times ($T = 5$), the velocity direction along the principal axis is almost opposite to the streamwise direction independent of the disturbance initial orientation. Consequently, local vertical shear layers, between the induced negative streamwise velocity and the base flow, are formed (e.g. see the vorticity sheets in figure 4*d* at $T = 5$). In the nonlinear case, the velocity field induced by the vortical structure has a significant vertical velocity component also at long times, leading to the injection of low-speed fluid into the high-velocity region. It is also evident that the velocity magnitude along the principal axis at long times associated with the

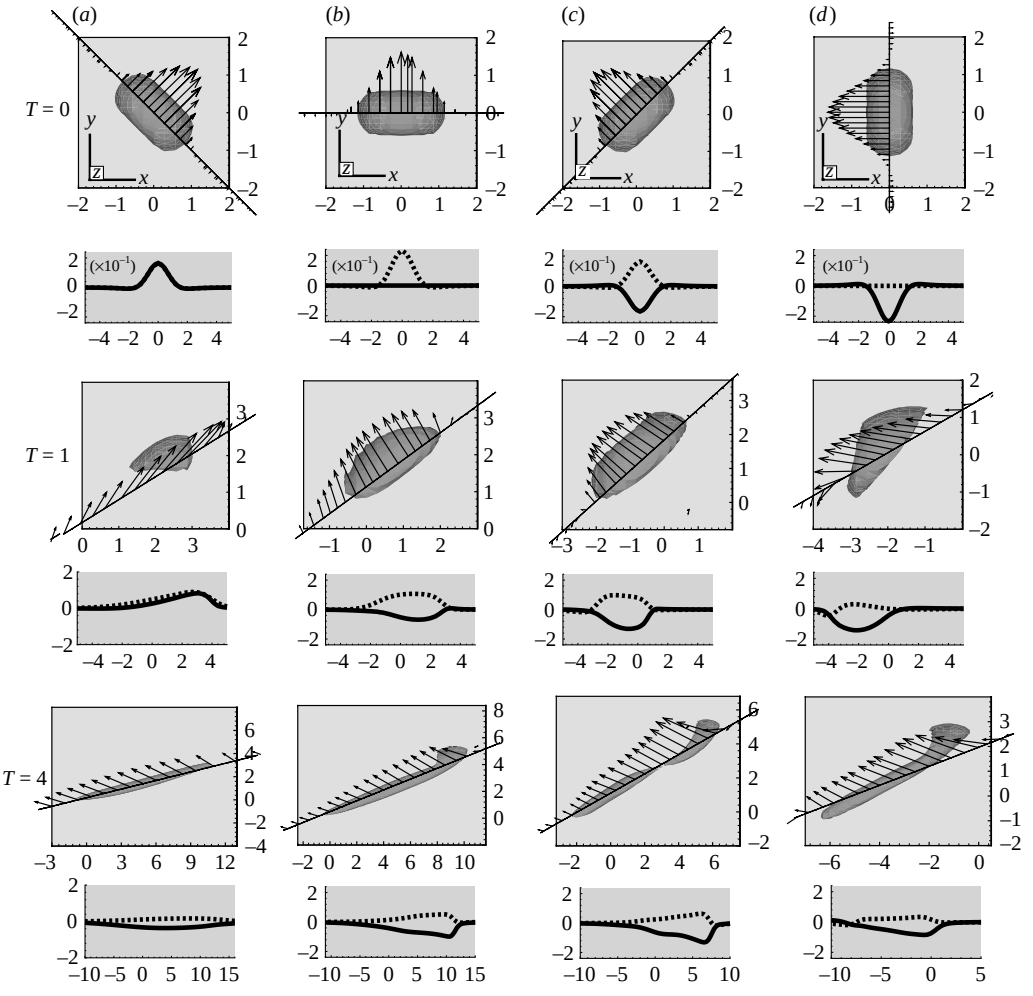

FIGURE 7. Evolution of a large-amplitude ($\varepsilon = 7.5$) disturbance. Odd rows: projection of the iso-surfaces of the vorticity magnitude for $||\boldsymbol{\omega}||/\omega_{max} = 0.7$ on the (x, y)-plane, long principal axis (black line), velocity vectors along the principal axis at the $Z = 0$ plane. Even rows: streamwise (solid) and vertical (dotted) velocity components ($\mathrm{m\,s^{-1}}$) distributions along the long principal axis at the $Z = 0$ plane. (The units along the abscissa correspond to $X/|\cos\alpha$.) (*a*) $\phi = 45^\circ$; (*b*) $\phi = 90^\circ$; (*c*) $\phi = 135^\circ$; (*d*) $\phi = 180^\circ$.

disturbance having $\phi = 45^\circ$ initial orientation is very weak in comparison with the disturbances having $\phi = 90^\circ$ or $\phi = 135^\circ$ initial orientations.

It should be noted that regardless of the initial small-amplitude disturbance orientation, the distributions of the velocity components along the principal axis remain symmetric around the origin during the entire evolution. This symmetry is due to the symmetry properties of both: the chosen initial disturbance and the linearized governing equations (Shukhman & Levinski 2003). In addition, the following trends can be observed during the linear disturbance evolution: (i) generation and growth of a negative streamwise velocity component and attenuation of the vertical velocity component for the disturbances initially having positive vertical velocity component; (ii) significant elongation of the disturbed velocity region. These findings suggest that the disturbance evolution is governed by the transient growth mechanism.

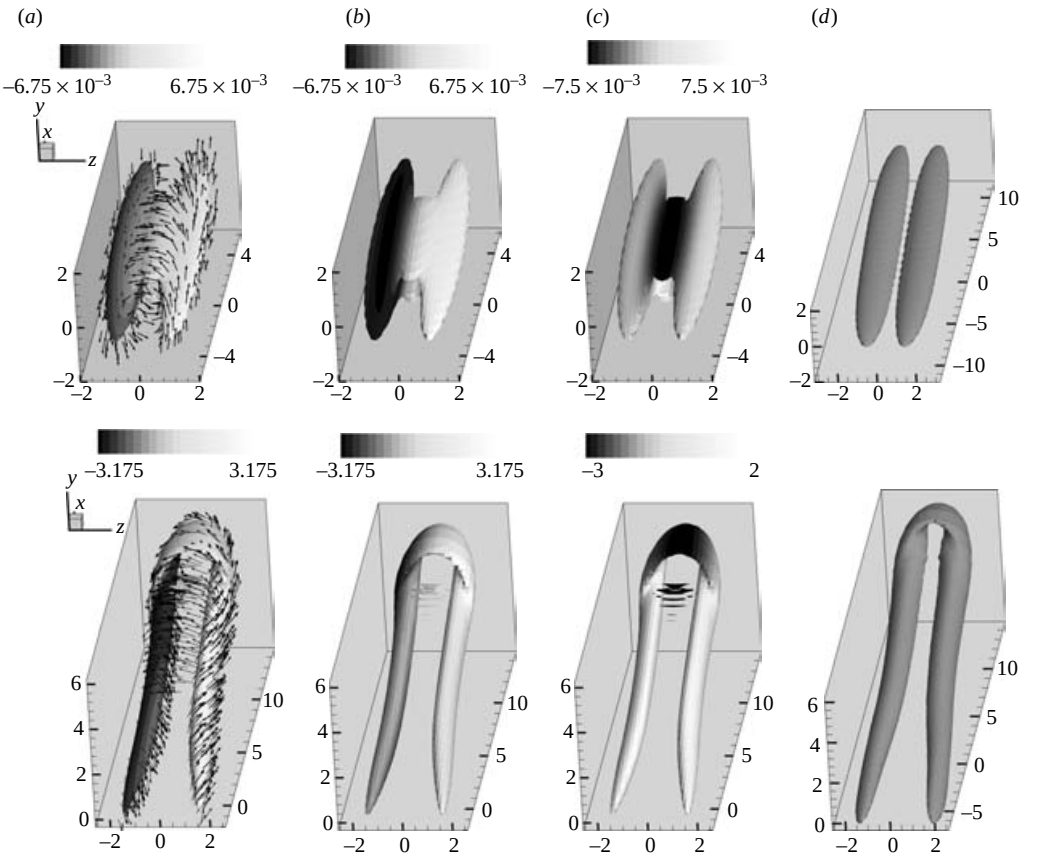

FIGURE 8. Top row: vortical structure developed from a small- ($\varepsilon = 0.015$) amplitude Gaussian vortex by $T = 5.75$. Bottom row: vortical structure developed from a large-amplitude ($\varepsilon = 7.5$) by $T = 5$. $\phi = 90°$, $Re = 40$. (*a–c*) Contours of ω_x, ω_y and ω_z vorticity components, respectively, shown on the iso-surface of the vorticity magnitude for $||\boldsymbol{\omega}||/\omega_{max} = 0.6$. (The values are normalized by the shear of the mean flow $\Omega = 40\,\mathrm{s}^{-1}$.) The associated vorticity vectors are shown by the black arrows. (*d*) Iso-surface according to the Q definition for $Q/Q_{max} = 0.05$.

From figure 7, it can be observed that, unlike the linear case (figure 6), the large-amplitude initial disturbance is shifted away from its initial position ($X = Y = 0$) by its self-induced motion. Thus, the direction of the initial movement, obviously depends on the disturbance initial orientation. Another significant difference with respect to the linear case, is that the distribution of the velocity components along the long principal axis loses its symmetry from the very beginning. Furthermore, once hairpin vortices begin to form, the maximum of the velocity magnitude is shifted towards the head of the hairpins.

In figure 8, the resulting vortical structure developed from a horizontal small- (top row) and large- (bottom row) amplitude Gaussian vortex is shown by the iso-surfaces of the vorticity magnitude and the Q definition. The contours of the corresponding three vorticity components are shown in figures 8(*a*), 8(*b*) and 8(*c*), respectively. The associated vorticity vectors are indicated in figure 8(*a*) by the black arrows. It can be seen that in the case of a small-amplitude disturbance, the top and bottom spanwise vorticity sheets, bridging the quasi-streamwise vortices, are not captured by the Q definition (figure 8*d*), as they do not contain swirling motion. These vorticity sheets

indicate the existence of local inclined shear layers, which are formed owing to the negative streamwise velocity induced by the vortical structure. Similar local shear layers are frequently observed in the near-wall region of a turbulent boundary layer. For the case of a large-amplitude disturbance, both methods extract similar vortical structures. With respect to the vorticity field it should be noted that in the linear case, the elongated regions of concentrated vorticity consist primarily of streamwise and vertical vorticity components, but the vertical component is the dominant one. Therefore, the direction of the vorticity vector strongly deviates from the direction of the vortical structure, and consequently in this case, the vortical structure cannot be represented as a vortex filament. Unlike the linear case, the vortical legs of the hairpin vortices contain all three vorticity components, whereas the head of the hairpin is dominated by the spanwise vorticity component. Consequently, the vorticity lines spiral around the vortical legs passing through the head of the hairpin. In comparison with the linear case, the vorticity lines follow much more closely the core of the vortical structure, resulting in a much stronger swirling motion around the legs and head of the hairpin. Therefore, in the nonlinear case, the deviation between the direction of the vorticity vector and the inclination angle of the vortical structure is much less significant in comparison with the linear case. This deviation was also observed by Bernard *et al.* (1993) in their DNS results of channel flow. Kida & Tanaka (1994) studied the evolution of concentrated vorticity regions in shear flow and reported that some differences between these two angles existed. For the initial vortical structure extracted from the DNS channel data by Zhou *et al.* (1999), the vorticity vector was inclined by $\approx 50^\circ$ relative to the streamwise direction, whereas the vortical structure itself was inclined only by $\approx 25^\circ$.

In order to examine carefully the effect of the initial disturbance amplitude on the evolutionary characteristics of the vortical structures, four initial amplitudes $\varepsilon = 0.015, 0.375, 3.75$ and 7.5 are considered. The disturbances having $\varepsilon = 0.015$ and 0.375 can be regarded as small-amplitude disturbances, i.e. their evolution is governed by the linearized equations (Suponitsky *et al.* 2004), whereas disturbances having $\varepsilon = 3.75$ and 7.5 initial amplitudes are considered as strong nonlinear disturbances. The fact that the evolution of relatively high-amplitude initial disturbances (upto $\varepsilon \approx 0.375$), is still governed by the linearized equations is due to the use of the vorticity ratio (ω_{max}/Ω) for the definition of the disturbance initial amplitude instead of the more conventional definition of the corresponding velocity ratio. For the latter case we have

$$\frac{u_{max}}{U_{base}} \approx \frac{\omega_{max}}{\Omega}\frac{\delta}{\Delta}, \tag{3.1}$$

where δ and Δ are the characteristic lengths scales of the disturbance and base flow, respectively. For localized disturbances (in all three dimensions), the characteristic length scales ratio can be assumed to be very small (Levinski & Cohen 1995). Consequently, the corresponding amplitude, expressed in terms of the velocities ratio is very small.

The effect of the initial amplitude on the evolution of the inclination angle α of the vortical structure for disturbances having initial orientations of $\phi = 90^\circ$ and $\phi = 135^\circ$ is presented in figures 9(*a*) and 9(*b*), respectively. For both initial orientations, the temporal evolution of the 'linear' disturbances with amplitudes $\varepsilon = 0.015$ and 0.375 is the same. However, for both cases, larger amplitudes of the initial disturbance result in larger inclination angles of the vortical structures during the entire evolution. Finally, examining the results of the horizontal ($\phi = 90^\circ$) initial disturbance, it can be

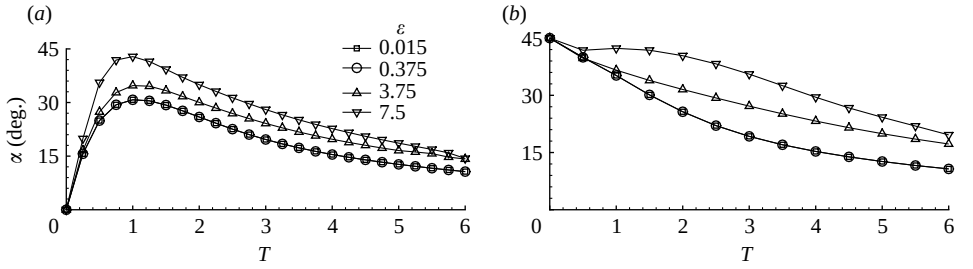

FIGURE 9. The effect of the initial amplitude on the temporal evolution of the inclination angle α for disturbances initially having different orientations: (*a*) $\phi = 90^\circ$; (*b*) $\phi = 135^\circ$.

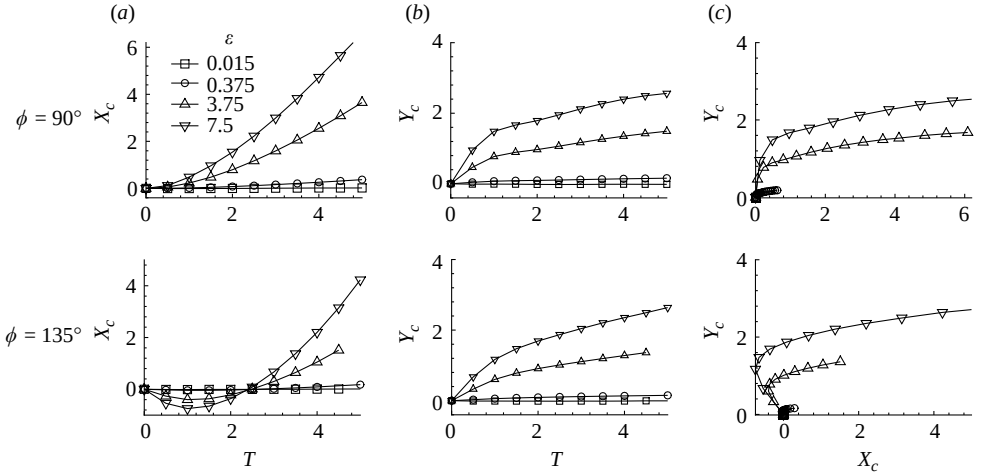

FIGURE 10. The effects of the disturbance initial amplitude and orientation on the CVS position (centre of the vortical structure). (*a*) X_c *vs.* T; (*b*) Y_c *vs.* T; (*c*) trajectory for $0 \leqslant T \leqslant 5$.

seen that independent of its initial amplitude, the maximum inclination angle of the vortical structure occurs at $T \approx 1$.

The difference between the linear and nonlinear disturbance evolutions is also evident when the effect of the disturbance initial amplitude on the position of its centre (CVS, see (2.10)) is considered. In figure 10, the temporal movement of the CVS for disturbances having $\phi = 90^\circ$ and $\phi = 135^\circ$ initial orientations and several amplitudes within the range of $0.015 \leqslant \varepsilon \leqslant 7.5$, is presented. The movement of the x-coordinate (X_c) and y-coordinate (Y_c) are shown in figures 10(*a*) and 10(*b*), respectively, whereas the corresponding trajectory is presented in figure 10(*c*). We can see that for the small-amplitude case ($\varepsilon = 0.015$), the CVS remains in its initial position ($X_c = Y_c = 0$) for both orientations of the initial disturbances. This is due to the symmetry properties of both: the chosen geometry of the initial disturbance and the linearized equations (Shukhman & Levinski 2003). The movement of the initial disturbance from its original position is a nonlinear effect caused by the self-induced velocity of the vortical structure and the destruction of the disturbance initial streamwise symmetry. The results show that for disturbances with the initial amplitude of $\varepsilon = 0.375$, only a slight movement of the CVS can be seen, owing to weak nonlinear effects, whereas for the stronger nonlinear disturbances ($\varepsilon = 3.75$ and 7.5), significant movement of the CVS is observed.

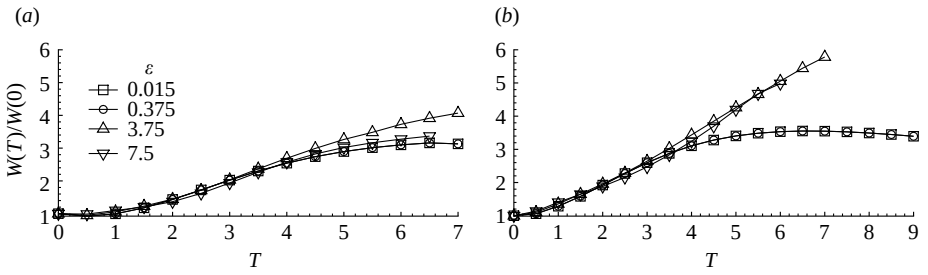

FIGURE 11. The effect of the initial disturbance orientation on the temporal evolution of the normalized enstrophy integral ($W(T)/W(0)$) for a range of amplitudes of the initial disturbance: $0.015 \leqslant \varepsilon \leqslant 7.5$. (*a*) $\phi = 90°$; (*b*) $\phi = 135°$.

As the base flow does not have a vertical velocity component, the vertical displacement of the CVS is due to the vortex self-induced velocity. Once the initial vortex is displaced in the vertical direction, its streamwise velocity includes the local streamwise base-flow velocity in addition to its streamwise self-induced velocity. The nonlinear initial disturbances, initially oriented at $\phi = 90°$ and $\phi = 135°$, have a significant positive vertical velocity component, leading to their rapid movement (which is proportional to their initial amplitude) of the vortical structures in the vertical direction at early stages of their evolution. Later on ($T > 1$), the movement of the CVS in the vertical direction varies approximately linearly with time, implying that the vertical velocity of CVS is approximately constant. Estimating $\mathrm{d}X_c/\mathrm{d}t$ at these times, the streamwise velocity of the CVS relative to the local base flow velocity can be calculated. Its value is found to be within the range of $0.65 \leqslant u_{cvs}/U_{base} \leqslant 0.75$. The defect of the CVS velocity relative to the local streamwise base-velocity (U_{base}) is due to the self-induced velocity, which by these times has a significant opposite component relative to the base-flow velocity.

In this respect, it is worth mentioning some relevant experimental results: Acarlar & Smith (1987*b*) reported that in the outer part of a laminar boundary layer, the velocity of the artificially generated hairpin's head is about 0.86 of the free-stream velocity (the value of the actual local velocity is not given). Smith (1978) investigated turbulent boundary layers and observed that outer-region disturbances with convection velocities of 0.60–$0.70U_\infty$ seemed to be those most associated with the lift-up of wall-region fluid. Svizher & Cohen (2002) studied the formation of hairpin vortices in sub-critical plane Poiseuille flow and reported that the velocity of the hairpin's head relative to the local base-velocity is between 0.65 and 0.75. Finally, examining the trajectory of the centre of the vortical structure (figure 10*c*), it can be seen that after some transient time, the trajectories of strongly nonlinear initial disturbances follow approximately linear curves. The slope of these curves is about 11°–12°, independent of the disturbance initial amplitude.

The temporal evolution of the normalized integral of enstrophy for disturbances having $\phi = 90°$ and $\phi = 135°$ initial orientations and amplitudes within the range of $0.015 \leqslant \varepsilon \leqslant 7.5$ is presented in figures 11(*a*) and 11(*b*), respectively. It can be seen that a significant growth is achieved by the nonlinear initial disturbances ($\varepsilon = 3.75$ and 7.5) having $\phi = 135°$ initial orientation. The nonlinear disturbances deviate from the linear ones at $T \approx 4$, where they continue to grow at the same rate, achieving an amplification factor of about 5 by $T \approx 5.5$. On the other hand, the growth rate of the linear disturbances is decreased (due to viscous effects) and they achieved their maximum amplification (about 3.5) at $T \approx 5.5$. A similar deviation, but not as

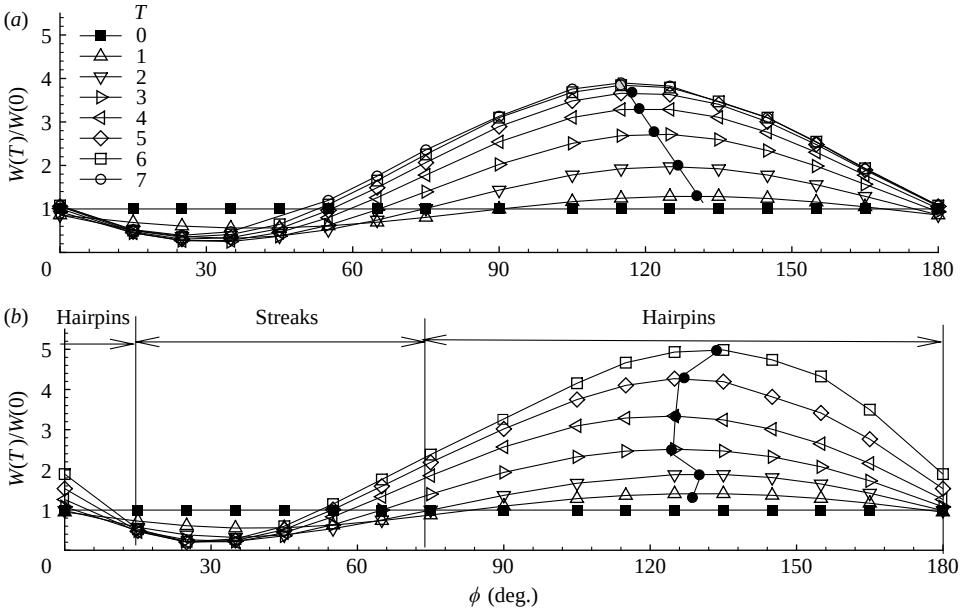

FIGURE 12. The effect of the initial disturbance orientation on the temporal evolution of the normalized enstrophy integral ($W(T)/W(0)$). (a) $\varepsilon = 0.375$ (linear case); (b) $\varepsilon = 7.5$ (nonlinear case).

sharp, can also be observed for disturbances having $\phi = 90^\circ$ initial orientation, but at later times. In this respect, it should be recalled that the strength of the vortical structure developed from a localized disturbance embedded in uniform shear base flow, is governed by the transient (algebraic for the inviscid case) growth mechanism (e.g. Ellingsen & Palm 1975; Landahl 1975; Benney & Gustavsson 1981). This growth is due to the growth of the streamwise disturbance velocity and the elongation of the vortical structure during the evolution. The term, responsible for the generation and growth of the streamwise velocity, is $v(\mathrm{d}U/\mathrm{d}y)$ (the lift-up term), which for positive normal velocity and $\mathrm{d}U/\mathrm{d}y$ leads to the generation of a negative streamwise velocity. As such, the initial orientation of the disturbance, i.e. the initial direction of the induced velocity relative to the base flow, is expected to have a drastic effect on the disturbance growth.

In light of the presented results, we wish to find the initial orientation which yields the maximum transient growth. For this purpose, simulations for two initial amplitudes $\varepsilon = 0.375$ (referred to as the linear case) and $\varepsilon = 7.5$ (referred to as the nonlinear case) are carried out, densely covering the whole range of initial orientations ($0 \leqslant \phi \leqslant 180^\circ$).

Figure 12 demonstrates the effect of the disturbance initial orientation on the temporal evolution of the normalized enstrophy integral. Figure 12(a) shows the linear case and figure 12(b) the nonlinear case. It can be seen that in both cases there is a range of initial orientations for which the strength of the vortex decreases and remains below its initial value during the entire evolution, whereas for all other orientations it increases. However, the disturbance growth rate depends on its initial orientation and amplitude. In the linear case (figure 12a), the strength of the vortex reaches a saturation level at $T \approx 6$, independent of the disturbance initial orientation. The initial orientation yielding the maximum growth of the vortical disturbance varies

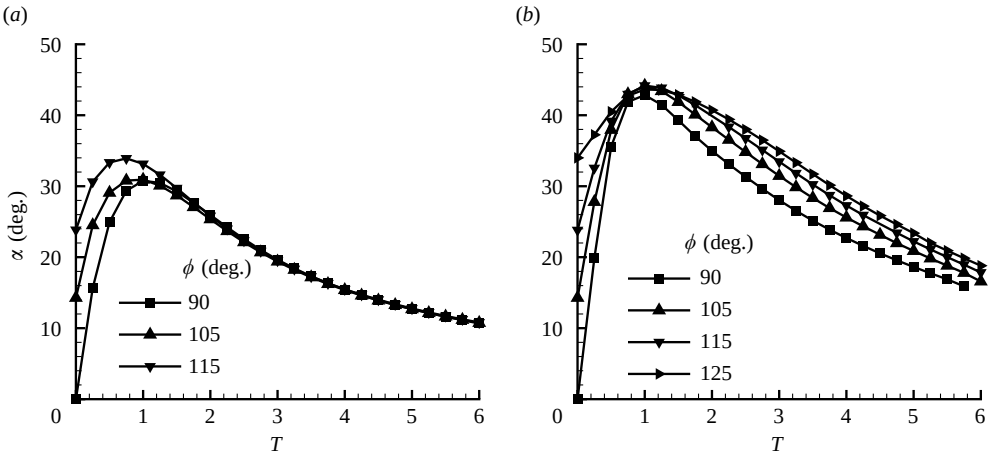

FIGURE 13. Temporal evolution of the vortical structure inclination angle α for disturbances having different initial orientations (angle ϕ) ($Re = 40$). (*a*) $\varepsilon = 0.375$, (*b*) $\varepsilon = 7.5$.

monotonically from $\phi \approx 130^\circ$ at $T = 1$ to $\phi \approx 115^\circ$ at $T = 7$. These results of the linear case agree very well with the analytic results obtained by Shukhman & Levinski (2003).

In the nonlinear case, the situation is quite different. There is a range of initial orientations, for which the integral of enstrophy continues to grow at approximately the same rate even at relatively long times ($T \approx 6$). The initial orientation, for which the vortex reaches its maximum strength, does not have a clear tendency during the evolution process. The most amplified disturbances have initial orientation within the range of $125^\circ \leqslant \phi \leqslant 135^\circ$.

Trying to understand the difference between the optimal orientation in the linear case ($\phi \approx 115^\circ$) and nonlinear ($\phi \approx 130^\circ$) cases, we now focus on the temporal evolution of the inclination angle α for the linear (figure 13*a*) and nonlinear (figure 13*b*) cases, respectively. As can be seen in figure 13(*b*), all disturbances reach a maximum inclination angle (α_{max}) by $T \approx 1$, before reversing their rotation. Note that the initial inclination angle for all of the disturbances shown in figure 13 is less than α_{max}. The value of α_{max} is close to 44° for the nonlinear case, and it is about 32° for the linear case. Thus, for a given geometry and an initial amplitude, the maximum inclination angle is approximately constant. The optimal disturbance can now be thought of as that having an initial inclination angle 'close' to α_{max}. In this case, the energy-consuming process of rotation is minimal. In this respect it should be mentioned that the value of $\alpha_{max} = 44^\circ$ for the nonlinear case, is within the range of inclination angles of hairpin vortices observed in turbulent boundary layers by various investigators (e.g. Head & Bandyopadhyay 1981) and to the predicted value of the model proposed by Levinski & Cohen (1995).

3.1.2. *The effect of the Reynolds number*

The effect of the Reynolds number was addressed in Suponitsky *et al.* (2004), where the inviscid analytic solution of the linearized vorticity equation (Shukhman & Levinski 2003) was compared to the analytic and numeric solutions for $Re = 40$. It was shown that the shape of the vorticity magnitude distribution is well preserved by the inviscid solution, whereas its actual magnitude is severely overestimated. To

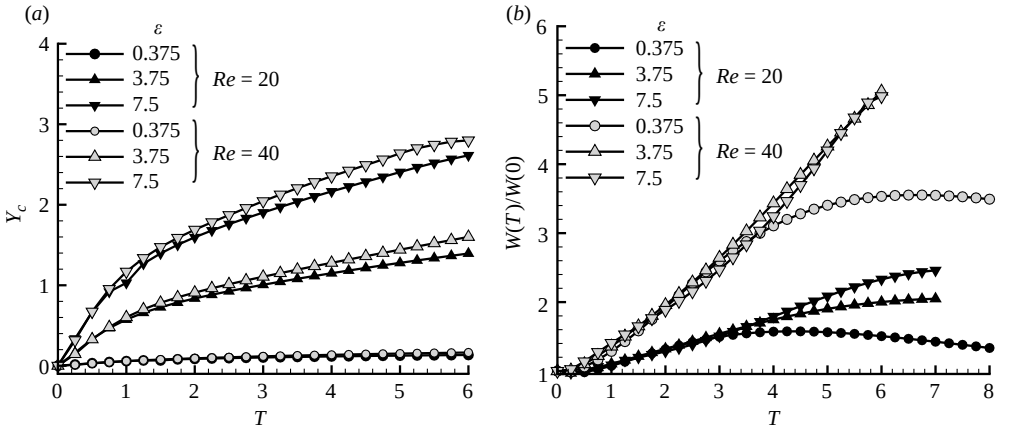

FIGURE 14. The effect of the Reynolds number ($\phi = 135°$). (*a*) Temporal evolution of the Y_c coordinate of the centre of the vortical structure; (*b*) temporal evolution of the normalized enstrophy integral ($W(T)/W(0)$).

complete the picture, the simulations for a Gaussian vortex disturbance, with an initial orientation of $\phi = 135°$, having different initial amplitudes are carried out for $Re = 20$ and the results are compared to those of $Re = 40$.

The results indicate that the Reynolds number has a negligible effect on the kinematics of the vortical structure. As an example the evolution of the Y_c coordinate of the centre of the vortical structure is shown in figure 14(*a*), demonstrating slight differences between the results associated with the two Reynolds numbers. However, the Reynolds number has a significant effect on the disturbance transient growth as is shown in figure 14(*b*).

First, it can be seen that for all initial amplitudes, the transient growth is significantly increased when the Reynolds number is doubled. For the small-(linear) amplitude disturbances, the ratio between the maximum strength of the vortical structure associated with $Re = 40$ and that of 20 is about 2.25, and the ratio of times by which these are attained is about 1.5. Both ratios agree well with the theoretical predictions concerning the linear case ($E_{max} \sim Re$ and $t_{max} \sim Re^{1/3}$, see table in the introduction of Bech *et al.* 1998).

3.1.3. *Asymmetric initial disturbances*

All the results presented so far have been confined to initial disturbances possessing initial spanwise symmetry. It has been shown that the spanwise symmetry for both small- and large-amplitude disturbances is conserved. In this respect, it is worth mentioning, that in the model proposed by Levinski & Cohen (1995), the evolution of a finite-amplitude localized disturbance is described in terms of the fluid impulse integral $\boldsymbol{p}$. Accordingly, the spanwise component of the fluid impulse remains equal to its initial value during the entire evolution. Consequently, if $p_z(T = 0) = 0$, the spanwise symmetry of the vortical structure is conserved.

In real flows, however, the perfect symmetry of the initial disturbance cannot be expected. Detailed analysis of DNS results (Spalart 1988; Robinson 1991) showed that the majority of hairpin vortices in the turbulent boundary layer are asymmetric (cane- and hook-like) hairpin vortices. To demonstrate the effect of the spanwise asymmetry of the initial disturbance, the evolution of a Gaussian vortex disturbance, initially

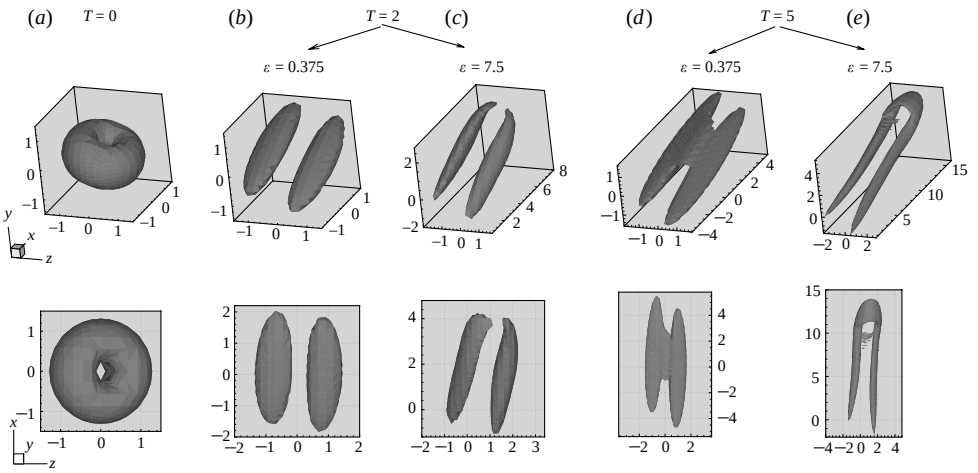

FIGURE 15. Evolution of small- ($\varepsilon = 0.375$) and large- ($\varepsilon = 7.5$) amplitude spanwise-asymmetric Gaussian-vortex disturbances ($\boldsymbol{p} = (0, |\boldsymbol{p}| \cos 20^\circ, |\boldsymbol{p}| \sin 20^\circ)$, $Re = 40$). First row: iso-surfaces of the vorticity magnitude for $||\boldsymbol{\omega}||/\omega_{max} = 0.6$; Second row: projection of iso-surfaces of the vorticity magnitude on the (x, z)-plane; (*a*) $T = 0$; (*b*) and (*c*) $T = 2$ for $\varepsilon = 0.375$ and $\varepsilon = 7.5$, respectively; (*d*) and (*e*) $T = 5$ for $\varepsilon = 0.375$ and $\varepsilon = 7.5$, respectively.

having a non-zero spanwise component of its associated fluid impulse, is considered. The simulations are carried out for the Gaussian vortex disturbance having an initial orientation of $\boldsymbol{p} = (0, |\boldsymbol{p}| \cos 20^\circ, |\boldsymbol{p}| \sin 20^\circ)$ (i.e. slightly rotated around the x-axis), for two initial amplitudes $\varepsilon = 0.375$ (small amplitude) and $\varepsilon = 7.5$ (strong nonlinear) and for $Re = 40$. The temporal evolutions of the small- and large-amplitude disturbances are plotted in figure 15. From this figure, it can be seen that the evolution (and the resulting structure) of a small-amplitude initial disturbance is very similar to that of a horizontal Gaussian vortex: the initial disturbance rotates about the z-axis and quickly evolves into two elongated, in the streamwise direction, vortical regions, which at long times are connected by spanwise vorticity sheets. However, the evolved vortical structure is not symmetric anymore relative to the $Z = 0$ plane: the elongated regions are shifted relative to each other in the streamwise and normal directions. Nevertheless, the structure remains almost symmetric relative to the origin ($X = Y = Z = 0$) owing to the symmetric properties of the linearized equations.

The evolution of the large-amplitude disturbance is also similar to that of the initially horizontal Gaussian vortex: the initial disturbance rotates about the z-axis and eventually evolves into a hairpin vortex. However, as a result of the spanwise asymmetry, the hairpin legs have different lengths and some asymmetries, associated with its head, can be observed. The movement of the vortical structure owing to its self-induced velocity in the spanwise direction (in addition to the x and y directions), can also be observed.

The above results demonstrate that even a slight spanwise asymmetry (20°) of the initial disturbances leads to a noticeable asymmetry of the resulting structure. Thus, the existence of asymmetric hairpins and hook-like vortices in fully turbulent flows may be explained by 'imperfection' of the initial disturbances (and/or the base flow). This point was also addressed in Zhou *et al.* (1999). Finally, it should be noted, that in real flows the variation of the base shear in the normal direction enhances the spanwise asymmetry of the initial disturbance.

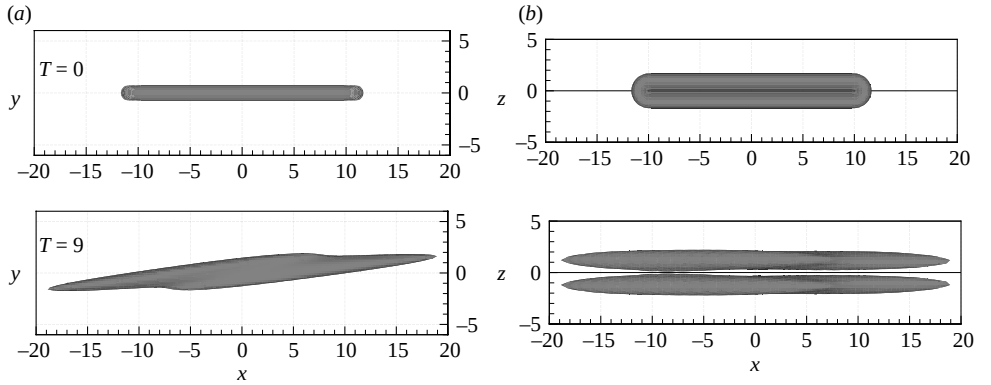

FIGURE 16. Top row: An initial small-amplitude streamwise elongated Gaussian disturbance ($L/\delta = 10$, $\varepsilon = 0.1125$, $Re = 40$ and $\phi = 90°$). Bottom row: resulting structure at $T = 9$. Projection of the Q-definition iso-surfaces for $Q/Q_{max} = 0.1$: (*a*) (x, y)-plane; (*b*) (x, z)-plane.

3.2. *Streamwise elongated disturbance*

3.2.1. *The effect of the streamwise disturbance elongation on the evolution of a small-amplitude initial disturbance*

In this section, the effect of the length scales ratio L/δ on the evolution of a small-amplitude initial disturbance is studied. All other parameters are held constant; the initial amplitude and orientation are $\varepsilon = 0.1125$ and $\phi = 90°$, respectively, and the Reynolds number is 40. The length scales ratio L/δ varies within the range $0 \leqslant L/\delta \leqslant 10$. The qualitative evolution of the disturbance and the resulting vortical structure are found to be sufficiently independent of the length scales ratio L/δ, and are similar to that of the horizontal Gaussian vortex (figure 4). The disturbance rotates around the z-axis and finally evolves into two streamwise elongated vortical regions, inclined at a small angle of $\alpha < 10°$. The induced velocity is mainly in the negative direction of the x-axis, which leads to the formation of a low-speed streaky structure. This resulting structure remains symmetric around the origin ($X = Y = Z = 0$) during the entire evolution owing to the symmetric properties of linearized equations and convected with the local velocity of the base flow (which is zero in our case). An example of the resulting structure, for which $L/\delta = 10$, is shown in figure 16 by the projections of the Q-definition iso-surfaces on the (x, y)- and (x, z)-planes, respectively. The development of the symmetric varicose instability mode (see for example Asai *et al.* 2002; Svizher & Cohen 2002; Skote *et al.* 2002) is evident from the Q-definition iso-surfaces on the (x, z)-plane for $T = 9$.

Despite the fact that the streamwise elongation of the initial disturbance has a relatively small effect on its qualitative evolutionary process, it has a significant effect on its quantitative characteristics (i.e. its inclination angle and transient growth). The temporal evolution of the inclination angle α for several disturbances having different length scales ratio L/δ is shown in figure 17. The maximum inclination angle (of about 30°) is attained by the Gaussian vortex at the shortest time ($T \approx 1$). When the ratio L/δ is increased, the time at which the maximum inclination angle is attained is increased, whereas the value of the angle itself is decreased. For a disturbance having a length scales ratio of $L/\delta = 10$ (which may be considered approximately as a 'streamwise independent' disturbance), the rate of rotation is very slow, such that by $T = 9$ the inclination angle is only about 5°.

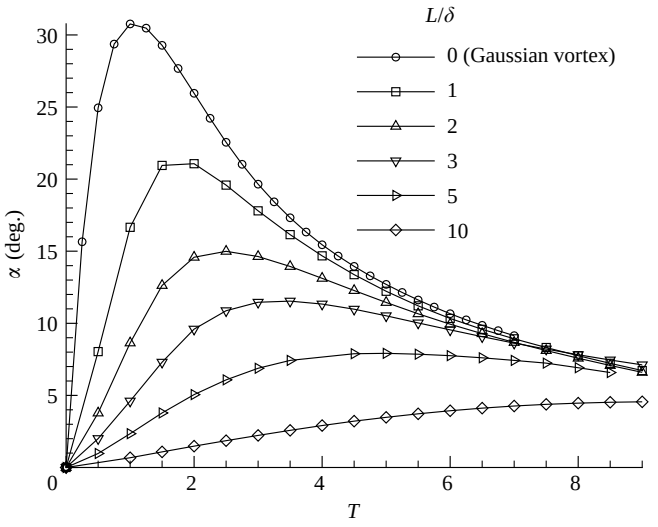

FIGURE 17. Temporal evolution of the vortical structure inclination angle α ($\varepsilon = 0.375$ for the Gaussian vortex and $\varepsilon = 0.1125$ for all others, $\phi = 90°$, $Re = 40$).

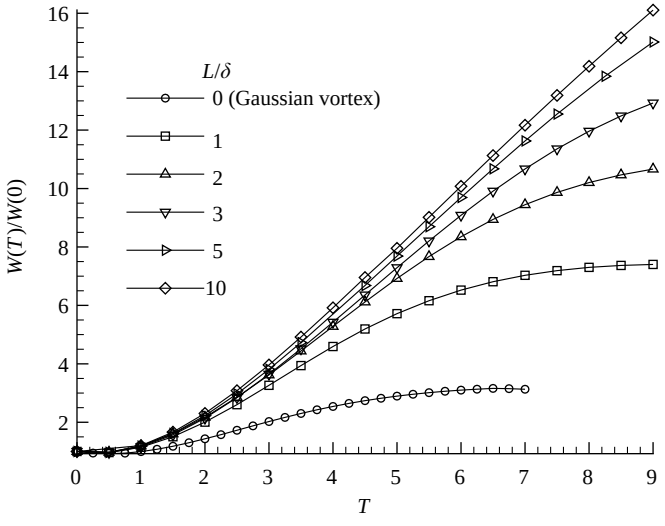

FIGURE 18. Temporal evolution of the normalized enstrophy integral ($W(T)/W(0)$) ($\varepsilon = 0.375$ for the Gaussian vortex and $\varepsilon = 0.1125$ for all others, $\phi = 90°$, $Re = 40$).

The temporal evolution of the normalized enstrophy integral is shown in figure 18. It can be seen that the geometry of the initial disturbance plays a very important role on its transient growth. The Gaussian vortex has the weakest growth, which attains its maximum (approximately 3.8) by $T \approx 6$, and then decays owing to viscous effects. Increasing the ratio L/δ results in a more significant transient growth which is attained at longer times. In comparison, the initial enstrophy integral for the disturbance having a length scales ratio of $L/\delta = 10$, is amplified by a factor of 16 by $T = 9$ and it still continues to grow. However, increasing the length scales ratio L/δ from 5 to 10, does not lead to a significant increase in the corresponding transient growth. It is not a

surprising result, because as the ratio L/δ is increased, the disturbance approaches the 'streamwise independent' state, for which the contributions of the disturbance end parts (front and rear) become negligible. This result qualitatively agrees with the 'linear' theoretical predictions, for which the transient growth of a streamwise independent disturbance is larger than that of a localized disturbance (Bech *et al.* 1998).

3.2.2. *The effect of the initial amplitude*

To examine the effect of the ratio L/δ on the evolution of strong initial disturbances, simulations are carried out for disturbances having an initial amplitude of $\varepsilon = 7.5$ and several length scales ratios ($L/\delta = 1$, 2, 3, 5 and 10). The results (not all presented here) show, that up to a certain ratio (of about $L/\delta \approx 5$), the disturbance evolution is similar to that of a Gaussian vortex, and the resulting structure is that of a single hairpin vortex. When the ratio L/δ is further increased, a packet of two or more hairpin vortices is formed. As two examples, the temporal evolution of streamwise elongated disturbances with $L/\delta = 5$ and 10, are presented in figure 19 by the projections of the Q-definition iso-surfaces on the (x, y)- and (x, z)-planes, respectively. The initial disturbance having a length scales ratio of $L/\delta = 5$ is placed at $X = 2$; $Y = -2$ in order to keep the vortex within the computational domain for sufficiently long times.

From figure 19, it is observed that the initial disturbance is convected in the positive vertical direction owing to its self-induced velocity. The downstream end of the disturbance is lifted up and its inclination angle increases during the evolution, forming a hairpin vortex. Another hairpin vortex, having an Ω-shape, is generated near the upstream end of the initial disturbance. For both length scales ratios, the resulting vortical structure is similar to the packet or street of hairpin vortices observed in different shear flows in numerous experimental and numerical studies (Acarlar & Smith 1987*a*, *b*; Zhou *et al.* 1999; Asai *et al.* 2002; Skote *et al.* 2002; A. Svizher, personal communication 2003).

The results show that for the 'nearly streamwise independent' disturbances (large L/δ ratios), the hairpin vortices are formed near the upstream and downstream disturbance ends, where the disturbance has a 'localized' character. At longer times, the 'streamwise independent' state of the middle part of the disturbance is broken owing to the influence of these edge-hairpins, leading to a possible formation of other hairpin vortices. Thus, for the formation of hairpin vortices, it is crucial for the vortex disturbance to have a localized structure. A further discussion on this issue is given in § 4. Finally, it is worth mentioning that, at long times, new quasi-streamwise vortices (similar to those reported by Acarlar & Smith 1987*b*; Zhou *et al.* 1999; Bernard *et al.* 1993) are generated below and to the sides of the primary vortical structure. These vortices are educed (but not shown here) and can be observed by extracting the vortical structure with a lower threshold level of the Q-definition iso-surfaces. Thus, although existing, the strength of these vortices is weak relative to the strength of the primary vortical structure.

3.3. *A brief description of the evolution of the toroidal vortex*

For the sake of completeness, in the following we briefly describe the evolution of the toroidal vortex (equation (2.4)). A detailed study can be found in Suponitsky *et al.* (2004). The toroidal disturbance is defined by two length scales r_o and δ, associated with the radius and the thickness of the torus, respectively. As the ratio r_o/δ is increased, the distance between the two vorticity maxima (along the z-coordinate) is increased, whereas the size of the regions having concentrated vorticity remains

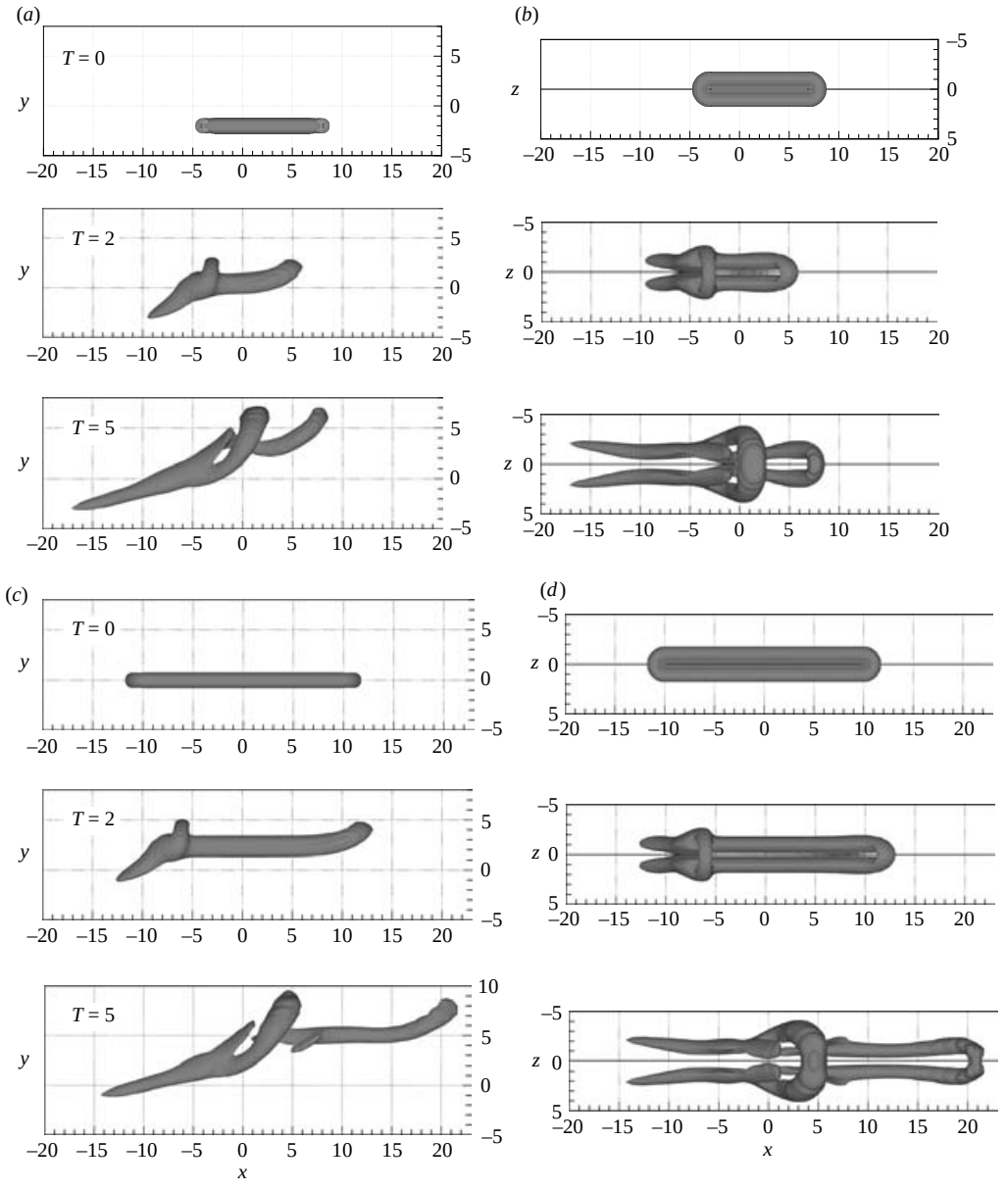

FIGURE 19. Temporal evolution of the streamwise elongated vortex disturbance with $L/\delta = 5$ and $L/\delta = 10$ length scales ratios ($\phi = 90°, Re = 40$). (*a*), (*c*) Projection of the Q-definition iso-surfaces on the (x, y)-plane for $L/\delta = 5$ and $L/\delta = 10$, respectively; (*b*), (*d*) projection of the Q-definition iso-surfaces on the (x, z)-plane for $L/\delta = 5$ and $L/\delta = 10$, respectively.

approximately the same (see figure 20). The temporal evolution of the normalized enstrophy integral is shown in figure 21. It can be seen that increasing the ratio r_o/δ results in a more significant transient growth which is attained at longer times. For the disturbance with $r_o/\delta = 5$–7 the initial enstrophy integral is amplified by a factor of about 22 by $T = 12$ and it still continues to grow. However, a further increase of the length scales ratio r_o/δ results in the reduction of the transient growth. Thus,

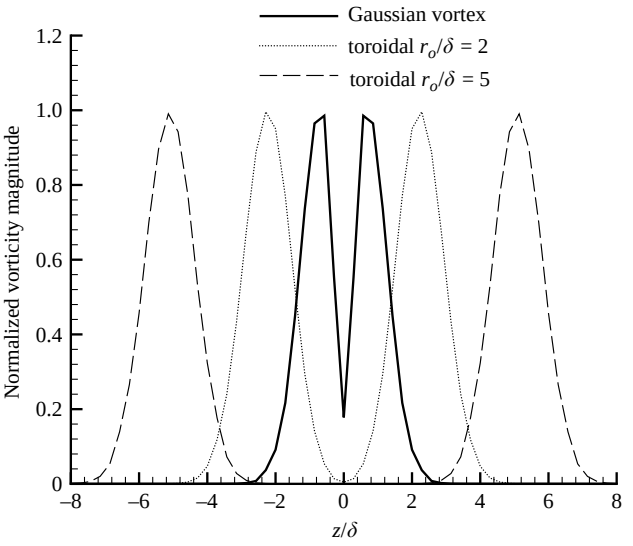

FIGURE 20. Normalized vorticity magnitude distribution along the z-axis for different geometrical shapes.

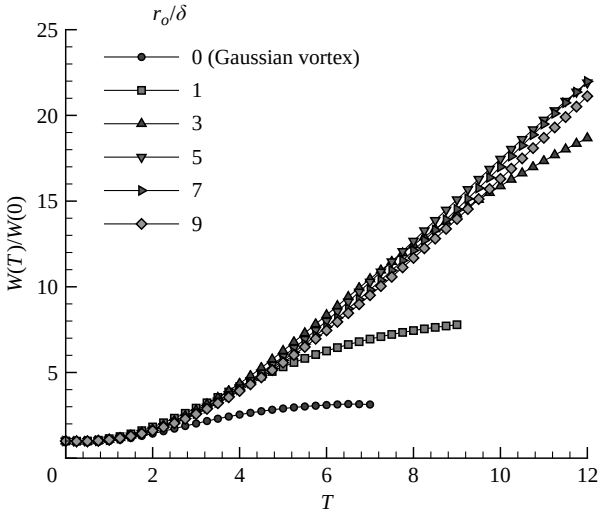

FIGURE 21. Temporal evolution of the normalized enstrophy integral ($W(T)/W(0)$) for different geometrical shapes ($\varepsilon = 0.375$, $\phi = 90°$, $Re = 40$).

the initial disturbances with length scales ratio within the range of $r_o/\delta = 5$–7, are 'optimal', i.e. they lead to the maximum transient growth. In this range, the separation distance between the two vorticity maxima ($\approx 2r_o$), expressed in terms of wall units, lies within the range of $63 \leqslant y^+ \leqslant 88$. In this respect, it should be noted that in turbulent boundary layers, the spanwise spacing between low-speed streaks is about 100 wall units and between hairpin legs is usually about 50–60 wall units and does not exceed 100.

In order to physically understand the existence of an optimal spanwise separation distance, we recall that the initial toroidal disturbance resembles a dipole

configuration. For such dipole configurations, the radius of each leg ($\approx\delta$) must be smaller than the distance between the centres of the two legs ($\approx 2r_o$). Otherwise, viscous diffusion can lead to vorticity cancellation and to the elimination of the vortex. On the other hand, when the spanwise separation distance is too large, the vortex loses its dipole structure, and consequently, the vortex strength is decreased.

4. Discussion

To further clarify the results and to understand better various aspects associated with the disturbance evolution, the disturbance vorticity equation (for the uniform shear base flow) is considered:

$$\frac{\partial \boldsymbol{\omega}}{\partial t} = \left[-\underbrace{(\boldsymbol{U}\cdot\nabla)\boldsymbol{\omega}}_{1} - \underbrace{(\boldsymbol{u}\cdot\nabla)\boldsymbol{\omega}}_{2} \right] + \left[\underbrace{(\boldsymbol{\omega}\cdot\nabla)\boldsymbol{U}}_{3} + \underbrace{(\boldsymbol{\Omega}\cdot\nabla)\boldsymbol{u}}_{4} + \underbrace{(\boldsymbol{\omega}\cdot\nabla)\boldsymbol{u}}_{5} \right] + \underbrace{\nu\nabla^2\boldsymbol{\omega}}_{6}, \qquad (4.1)$$

where $\boldsymbol{\omega} = \nabla \times \boldsymbol{u}$ is the finite-amplitude vorticity disturbance field and $\boldsymbol{\Omega} = \nabla \times \boldsymbol{U}$ is the shear of the base flow. Terms (1) and (2) in (4.1) represent the advection of the disturbance vorticity, without changing the direction of its associated vorticity vector. Terms (3), (4) and (5) are responsible for the tilting and stretching of the vorticity lines, and subsequent change of the direction or intensity of the vorticity vector. Term (1) is a linear term representing the rotation of the vortical structure by the mean shear. For uniform shear base flow it is equal to $-\Omega y(\partial\omega_i/\partial x)$. Term (2) is a nonlinear term and therefore, it has a negligible effect on the evolution of small-amplitude disturbances. It can be seen that the 'sign' and magnitude of term (1) depend on the initial vorticity distribution (i.e. the shape and orientation of the initial disturbance). For example, for Gaussian vortex disturbances having $\phi = 45^\circ$ and $\phi = 135^\circ$ initial orientations, the x-derivatives of ω_x and ω_z vorticity components are identical, but the associated x-derivatives of ω_y have the same magnitude but opposite signs, leading to different evolutionary processes. For the initially horizontal Gaussian and streamwise elongated disturbances, the signs of the x-derivatives of the vorticity components are the same, but the gradients of the vorticity in the streamwise direction are decreased as the length scales ratio L/δ is increased, leading to slower and weaker rotation of the vortical structure. For the disturbances with large L/δ length scales ratios, the rotation process begins near both ends of the disturbance, where the disturbance has a 'localized character' (i.e. localized gradients in the streamwise direction). Thus, as the disturbance approaches the 'streamwise independent' state, its ability to rotate is reduced.

Term (1) is responsible for the convection of the vorticity components (in a similar manner by which a passive scalar is convected). Each of the vorticity components is convected by the uniform-shear base flow, such that it seems that the region of the concentrated vorticity rotates around the z-axis. This point is illustrated in figure 22 for a Gaussian vortex disturbance having $\phi = 90^\circ$, $Re = 40$ and $\varepsilon = 0.375$. In figure 22(a), the projection on the (x, y)-plane of the vorticity magnitude iso-surfaces is presented. The contours of the vorticity magnitude (figure 22b) and the x, y and z vorticity components (shown, respectively, in figures 22c–22e) are presented for the cross-section plane $Z = 0.71$, the plane where the maximum voticity magnitude is attained. We can see the deformation of the x-vorticity component (figure 22c) caused by the first term (term(1)), generation and subsequent deformation of the y-vorticity component (figure 22d), deformation and attenuation of the z-vorticity component associated with the initial disturbance (figure 22e up to $T = 2$), and subsequent generation of the z-vorticity component, corresponding to the spanwise

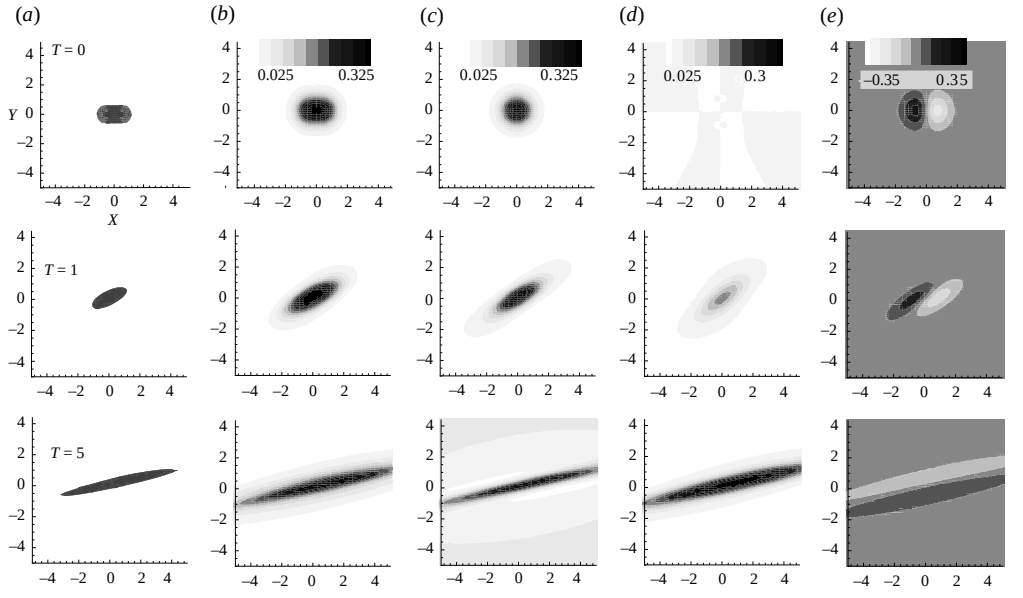

FIGURE 22. Evolution of a Gaussian vortex disturbance ($\phi = 90°$, $Re = 40$, $\varepsilon = 0.375$). (a) Projection on the (x, y)-plane of the vorticity magnitude iso-surface for $||\boldsymbol{\omega}||/\omega_{max} = 0.7$; ($b$) contours of the vorticity magnitude; (c) contours of the x-vorticity component; (d) contours of the y-vorticity component; (e) contours of the z-vorticity component. Contours (b–e) are presented at the $Z = 0.71$ plane, the plane where the maximum voticity magnitude is attained.

vorticity sheets (note the change of signs between $T = 1$ and $T = 5$). The resulting rotation of the high vorticity region caused by the convective term (1) is shown in figure 22(a, b).

Figure 23 follows the same structure as that of figure 22 for the streamwise elongated disturbance having length scales ratio of $L/\delta = 1$ and amplitude of $\varepsilon = 0.1125$. This figure demonstrates that the deformation of the concentrated vorticity region begins from the upstream and downstream 'edges' of the initial disturbance, where the disturbance has a localized character. At later stages of the evolution ($T > 1$), the deformation of the 'edges' affects the 'streamwise independent' middle part, leading (again) to the rotation of the entire concentrated vorticity region. Therefore, when the length of the 'streamwise independent' part is increased (i.e. increasing the ratio L/δ), a longer time is required before the whole disturbance is deformed by the mean shear, resulting in a slower and a weaker rotation of the concentrated vorticity region.

As was mentioned earlier with regard to (4.1), the direction of the vortical structure on one hand, and the vorticity vectors on the other, are governed by different terms in the vorticity equation. Therefore, the correspondence between them is not obvious and depends on the balance between the different terms. The small-amplitude streamwise-independent disturbance serves as a good example. In this case, term (1) is equal to zero and therefore the disturbance does not rotate. However, because term (4) does not equal zero (as $\partial u_i/\partial z \neq 0$), the direction of the vorticity vector is changed.

The difference in the resulting geometrical shapes and the dynamics of the structures, evolved from linear and nonlinear initial disturbances, are due to the nonlinear terms in the disturbed vorticity equation (terms 2 and 5 in (4.1)). Term (2) represents the advection of the vorticity by the velocity induced by the disturbance itself (self-induced velocity). Term (5) represents the conversion from one vorticity

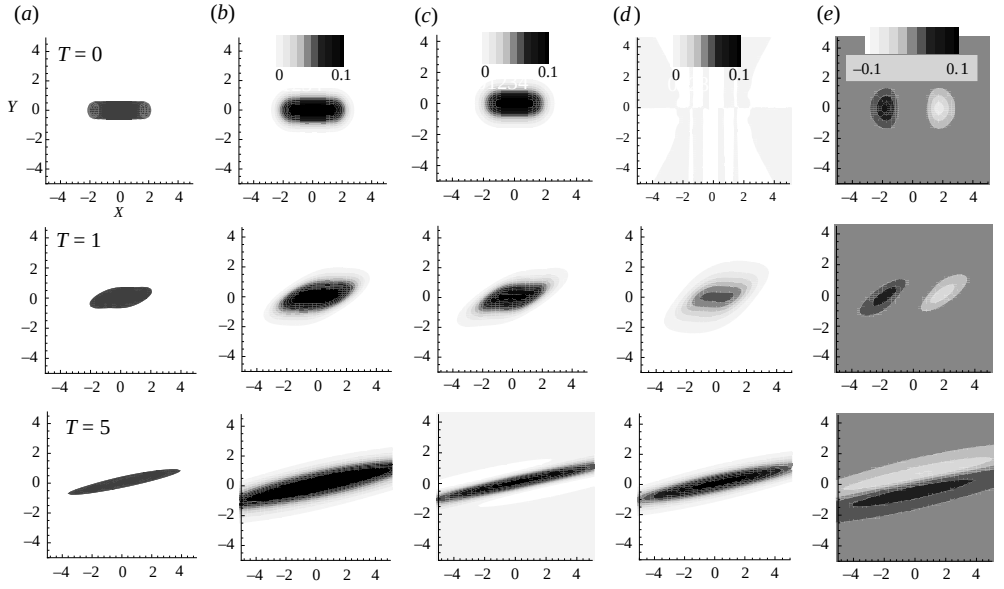

FIGURE 23. Evolution of a streamwise elongated disturbance ($L/\delta = 1$, $\phi = 90°$, $Re = 40$, $\varepsilon = 0.1125$). (*a*) Projection on the (x, y)-plane of the vorticity magnitude iso-surface for $||\boldsymbol{\omega}||/\omega_{max} = 0.7$; (*b*) contours of the vorticity magnitude; (*c*) contours of the x-vorticity component; (*d*) contours of the y-vorticity component; (*e*) contours of the z-vorticity component. Contours (*b–e*) are presented at the $Z = 0.71$ plane, the plane where the maximum vorticity magnitude is attained.

component to another, or the change of intensity of the vorticity vector by stretching or contraction of the vorticity lines. As was pointed out by Hunt (2000), the growth rate of term (5) is relatively slow, as the velocity gradients are decreased owing to the stretching of the vortical structure. Therefore, the most significant nonlinear effect (at least at relatively short times) is due to term (2). Our results for the Gaussian vortex demonstrate this very clearly. Owing to its self-induced motion (term 2), the disturbance with $\varepsilon = 0.375$ is moved from its initial position and its streamwise symmetry is broken (in comparison to $\varepsilon = 0.015$). At the same time, the normalized enstrophy integral is almost identical for both amplitudes, and a significant difference is only observed (at longer times) for much larger initial-amplitude disturbances.

5. Conclusions

A simple model, which takes into account only the interaction between a localized vortical disturbance and a laminar uniform shear base flow, is capable of reproducing the generation process and characteristics of coherent structures (streaks and hairpin vortices), naturally occurring in fully developed wall-bounded turbulent shear flows.

Streaks and hairpins. The results demonstrate that independent of the initial disturbance geometry and over a wide range of the initial disturbance orientations, a small-amplitude vortical disturbance eventually evolves into a pair of streamwise vortices (and corresponding streaks), whereas, a sufficiently large-amplitude disturbance evolves into a hairpin vortex (or a packet of hairpin vortices).

Spanwise spacing. The results (limited, however, to small-amplitude toroidal disturbances) show that there is an 'optimal' range of length scales ratios ($r_o/\delta = 5$–7)

for which the transient growth is the largest. In this 'optimal' range, the spanwise separation between the two elongated vortical regions, expressed in terms of wall units (60–90), corresponds well to the spanwise spacing of the low-speed streaks observed in turbulent bounded shear flows.

Inclination angle. For the large-amplitude initial Gaussian vortex, optimal disturbances are those having an initial inclination angle of about 45° ($\phi \approx 135°$). This value is within the range of inclination angles of hairpin vortices observed in turbulent boundary layers.

Convective velocity. The convective velocity of the vortical structures evolved from large-amplitude disturbances is found to be between $0.65 \leqslant u_{cvs}/U_{base} \leqslant 0.75$, which is in good agreement with corresponding reported values measured in wall-bounded turbulent shear flows.

Asymmetric hairpin vortices. The results show that a slight spanwise asymmetry of the initial vortex disturbance can lead to significant asymmetry of the evolved hairpin vortex. This result may explain the existence of asymmetric vortical structures frequently reported in real turbulent flows, unlike the symmetric ones which are usually observed in sub-critical flows studies.

For the small-amplitude disturbances there is a strong deviation between the vorticity vector and the direction of the resulting vortical structure. Consequently, in this 'linear' case, the vortical structure cannot be represented as a vortex filament. This deviation is much less significant in the 'nonlinear' case of a large-amplitude disturbance. In the latter case, the vorticity lines are more collapsed, resulting in a much stronger swirling motion around the legs and head of the hairpin.

The generation (and development) of hairpin vortices is initiated in regions where the disturbance possesses a 'localized' character (i.e. localized gradients in the streamwise direction). Accordingly, the generation of a 'street' or packet of hairpin vortices from a streamwise independent initial disturbance, seems unlikely, unless it is subjected to a secondary instability, or affected by the streamwise edges of the disturbance.

The Reynolds number has a negligible effect on the kinematics of the vortical structure (i.e. its CVS position and inclination angle), but has a significant effect on its transient growth.

We would like to thank Professor Ilia Shukhman and Dr Vladimir Levinski for the fruitful discussions and collaboration during the first stages of the research, for providing us with all the details of their analytical solution and the description of the tensor of enstrophy distribution (TED), which allows us to make a detailed validation of our numerical results.

This research has been supported by the Israeli Science Foundation under Grant no. 412/00.

REFERENCES

Acarlar, M. S. & Smith, C. R. 1987*a* A study of hairpin vortices in a laminar boundary layer. Part 1. Hairpin vortices generated by a hemisphere protuberance. *J. Fluid Mech.* **175**, 1.

Acarlar, M. S. & Smith, C. R. 1987*b* A study of hairpin vortices in a laminar boundary layer. Part 2. Hairpin vortices generated by fluid injection. *J. Fluid Mech.* **175**, 43.

Adrian, R. J., Meinhart, C. D. & Tomkins, C. D. 2000 Vortex organization in the outer region of the turbulent boundary layer. *J. Fluid Mech.* **422**, 1.

Andersson, P., Berggren, M. & Henningson, D. S. 1999*a* Optimal disturbances and bypass transition in boundary layers. *Phys. Fluids* **11**, 134.

Andersson, P., Brandt, L., Bottaro, A. & Henningson, D. S. 2001 On the breakdown of boundary layer streaks. *J. Fluid Mech.* **428**, 29.

Asai, M., Minagawa, M. & Nishioka, M. 2002 The instability and breakdown of a near-wall low-speed streak. *J. Fluid Mech.* **455**, 289.

Batchelor, G. K. 1967 *An Introduction to Fluid Dynamics*. Cambridge University Press.

Bech, K. H., Henningson, D. S. & Henkes, R. A. W. M. 1998 The linear and nonlinear development of localized disturbances in zero and adverse pressure gradient boundary-layers. *Phys. Fluids* **10**, 1405.

Ben-Dov, G., Levinski, V. & Cohen, J. 2003 On the mechanism of optimal disturbances: the role of a pair of nearly parallel modes. *Phys. Fluids* **15**, 1961.

Benney, D. J. & Gustavsson, L. H. 1981 A new mechanism for linear and nonlinear hydrodynamic instability. *Stud. Appl. Maths* **64**, 185.

Bernard, P. S., Thomas, J. M. & Handler, R. A. 1993 Vortex dynamics and the production of Reynolds stress. *J. Fluid Mech.* **253**, 385.

Blackwelder, R. F. 1983 Analogies between transitional and turbulent boundary layer. *Phys. Fluids* **26**, 2807.

Boberg, L. & Brosa, U. 1988 Onset of turbulence in a pipe. *Z. Naturforschung* **43a**, 697.

Breuer, K. S. & Haritonidis, J. H. 1990 The evolution of a localized disturbances in a laminar boundary layer. Part 1. Weak disturbances. *J. Fluid Mech.* **220**, 569.

Breuer, K. S. & Landahl, M. T. 1990 The evolution of a localized disturbances in a laminar boundary layer. Part 2. Strong disturbances. *J. Fluid Mech.* **220**, 595.

Brooke, J. W. & Hanratty, T. J. 1993 Origin of turbulence-producing eddies in a channel flow. *Phys. Fluids* **5**, 1011.

Butler, K. M. & Farrell, B. F. 1992 Three-dimensional optimal perturbations in viscous shear flow. *Phys. Fluids* A **4**, 1637.

Chong, M. S., Perry, A. E. & Cantwell, B. J. 1990 A general classification of three-dimensional flow field. *Phys. Fluids* A **2**, 765.

Darbyshire, A. G. & Mullin, T. 1995 Transition to turbulence in constant-mass-flux pipe flow. *J. Fluid Mech.* **289**, 83.

Dauchot, O. & Daviaud, F. 1995 Finite amplitude perturbation and spots growth mechanism in plane Couette flow. *Phys. Fluids* **7**, 335.

Ellingsen, T. & Palm, E. 1975 Stability of linear flow. *Phys. Fluids* **18**, 487.

Elofsson, P. A. & Alfredsson, P. H. 1998 An experimental study of oblique transition in plane Poiseuille flow. *J. Fluid Mech.* **358**, 177.

Gustavsson, L. H. 1991 Energy growth of three-dimensional disturbances in plane Poiseuille flow. *J. Fluid Mech.* **224**, 241.

Haidari, A. H. & Smith, C. R. 1994 The generation and regeneration of single hairpin vortices. *J. Fluid Mech.* **277**, 135.

Hamilton, J. M., Kim, J. & Waleffe, F. 1995 Regeneration mechanisms of near-wall turbulence structures. *J. Fluid Mech.* **287**, 317.

Head, M. R. & Bandyopadhyay, P. 1981 New aspects of turbulent boundary-layer structure. *J. Fluid Mech.* **107**, 297.

Henningson, D. S., Lundbladh, A. & Johansson, A. V. 1993 A mechanism for bypass transition from localized disturbances in wall bounded shear flows. *J. Fluid Mech.* **250**, 169.

Hultgren, L. S. & Gustavsson, L. H. 1981 Algebraic growth of disturbances in a laminar boundary layer. *Phys. Fluids* **24**, 1000.

Hunt, J. C. R. 2000 Dynamics and statistics of vortical eddies in turbulence. In *Turbulence Structure and Vortex Dynamics* (ed. J. C. R. Hunt & J. C. Vassilicos), p. 192. Cambridge University Press.

Hunt, J. C. R., Wray, A. A. & Moin, P. 1988 Eddies, stream, and convergence zones in turbulent flows. *Centre for Turbulence Research, Stanford University, Report* CTR-S88, p. 193.

Jeong, J. & Hussain, F. 1995 On the identification of a vortex. *J. Fluid Mech.* **285**, 69.

Jimenez, J. & Moin, P. 1991 The minimal flow unit in near-wall turbulence. *J. Fluid Mech.* **225**, 213.

Jimenez, J. & Pinelli, A. 1999 The autonomous cycle of near-wall turbulence. *J. Fluid Mech.* **389**, 335.

Kida, S. & Tanaka, M. 1994 Dynamics of vortical structures in a homogeneous shear flow. *J. Fluid Mech.* **274**, 43.

Kim, H. T., Kline, S. J. & Reynolds, W. C. 1971 The production of turbulence near a smooth wall. *J. Fluid Mech.* **50**, 133.

Kim, J., Moin, P. & Moser, R. D. 1987 Turbulent statistics in fully developed channel flow at low Reynolds number. *J. Fluid Mech.* **177**, 133.

Kline, S. J., Reynolds, W. C., Schraub, F. A. & Runstadler, P. W. 1967 The structure of turbulent boundary layers. *J. Fluid Mech.* **30**, 741.

Landahl, M. T. 1975 Wave breakdown and turbulence, SIAM. *J. Appl. Maths* **28**, 735.

Landahl, M. T. 1980 A note on an algebraic instability of inviscid parallel shear flows. *J. Fluid Mech.* **98**, 243.

Leite, R. J. 1959 An experimental investigation of the stability of Poiseuille flow. *J. Fluid Mech.* **5**, 81.

Leutheusser, H. J. & Chu, V. H. 1971 Experiments on plane Couette flow. *J. Hydraul. Div. ASCE* **97**, 1269.

Levinski, V. & Cohen, J. 1995 The evolution of a localized vortex disturbance in external shear flows. Part 1. Theoretical considerations and preliminary experimental results. *J. Fluid Mech.* **289**, 159.

Luchini, P. 2000 Reynolds-number-independent instability of the boundary layer over a flat surface: optimal perturbations. *J. Fluid Mech.* **404**, 289.

Malkiel, E., Levinski, V. & Cohen, J. 1999 The evolution of a localized vortex disturbance in external shear flows. Part 2. Comparison with experiments in rotating shear flows. *J. Fluid Mech.* **379**, 351.

Panton, R. L. 1997 *Self-Sustaining Mechanisms of Wall Turbulence*. Computational Mechanics, Southampton.

Rayleigh, Lord 1880 *Scientific Papers* (*1899*), vol. 1, p. 474. Cambridge University Press.

Reddy, S. C. & Henningson, D. S. 1993 Energy growth in viscous channel flows. *J. Fluid Mech.* **252**, 209.

Reynolds, O. 1883 An experimental investigation of the circumstances which determine whether the motion of water shall be direct or sinuous and of the law of resistance in parallel channels. *Proc. R. Soc. Lond.* **35**, 84.

Robinson, S. K. 1991 Coherent motions in the turbulent boundary layers. *Annu. Rev. Fluid Mech.* **23**, 601.

Rosenfeld, M., Cohen, J. & Levinski, V. 1999 The effect of rotation on the growth of hairpin vortices in shear flows. In *Proc. of the First Intl Symp. on Turbulence and Shear Flow Phenomena* (ed. S. Banerjee & J. K. Eaton), p. 21. Bagell House.

Schoppa, W. & Hussain, F. 2002 Coherent structure generation in near-wall turbulence. *J. Fluid Mech.* **453**, 57.

Shukhman, I. G. & Levinski, V. 2003 Evolution of the three-dimensional localized vortices in shear flows. Linear theory. *Elektronnii Zhurnal 'Issledovano v Rossii'* (*in Russian*).

Singer, A. & Joslin, R. D. 1994 Metamorphosis of a hairpin vortex into a young turbulent spot. *Phys. Fluids* **6**, 3724.

Skote, M., Haritonidis, J. H. & Henningson, D. S. 2002 Varicose instabilities in turbulent boundary layers. *Phys. Fluids* **14**, 2309.

Smith, C. R. 1978 Visualization of turbulent boundary layer structure using a moving hydrogen buble wire probe. *Lehigh Workshop on Coherent Structure in Turbulent Boundary Layers*, pp. 48–49.

Smith, C. R. & Metzler, S. P. 1983 The characteristics of low-speed streaks in the near-wall region of a turbulent boundary layer. *J. Fluid Mech.* **129**, 27.

Smith, C. R. & Walker, J. D. A. 1995 Turbulent wall-layer vortices. *Fluid Mech. Applic.* **30**, 235.

Spalart, P. R. 1988 Direct numerical simulation of a turbulent boundary layer up to $Re_\theta = 1410$. *J. Fluid Mech.* **187**, 61.

Suponitsky, V. 2003 The generation of streaks and hairpin vortices from a localized vortex disturbance embedded in unbounded uniform shear flow. PhD thesis, Technion–Israel Institute of Technology.

Suponitsky, V., Cohen, J. & Bar-Yoseph, P. Z. 2003*a* The development of a localized vortex disturbance in uniform shear flow – The effect of the initial amplitude. In *Proc. of the*

43rd Israel Annual Conf. on Aerospace Sciences (also available at: http://tx.technion.ac.il/~/cml/cml/staff/vika.htm).

Suponitsky, V., Cohen, J. & Bar-Yoseph, P. Z. 2003*b* The development of a localized vortex disturbance in uniform shear flow – The effect of the initial orientation. In *Proc. of the 29th Israel Conf. on Mechanical Engineering* (also available at: http://tx.technion.ac.il/~/cml/cml/staff/vika.htm).

Suponitsky, V., Cohen, J. & Bar-Yoseph, P. Z. 2004 Evolution of localized vortex disturbance in uniform shear flow: Numerical investigation. *AIAA J.* **42**, 1122.

Svizher, A. & Cohen, J. 2002 The evolution of hairpin vorticea in sub-critical air channel flow. In *Proc. of the Ninth European Turbulence Conf.* (ed. I. P. Castro, P. E Hancock and T. G. Thomas), p. 107. CIMNE.

Swearingen, J. D. & Blackwelder, R. F. 1987 The growth and breakdown of streamwise vortices in the presence of a wall. *J. Fluid Mech.* **182**, 255.

Tillmark, N. & Alfredsson, P. H. 1992 Experiments on transition in plane Couette flow. *J. Fluid Mech.* **235**, 89.

Wallace, J. M. 1985 *The Vortical Structure of Bounded Turbulent Shear Flow*. (ed. G. E. A. Meier and F. Obermeier). Lecture Notes in Physics, vol. 135, p. 253. Springer.

Wygnanski, I. J. & Champagne, F. H. 1973 On transition in a pipe. Part 1. The origin of puffs and slugs and the flow in turbulent slug. *J. Fluid Mech.* **59**, 281.

Zhou, J., Adrian, R. J. & Balachandar, S. 1996 Autogeneration of near wall vortical structure in channel flow. *Phys. Fluids* **8**, 288.

Zhou, J., Adrian, R. J., Balachandar, S. & Kendall, T. M. 1999 Mechanism for generating coherent packets of hairpin vortices in channel flow. *J. Fluid Mech.* **387**, 353.